UNIVERSITY OF CALIFORNIA, SAN DIEGO

Untangling the Ganglion: Connectomics in the Medicinal Leech

A dissertation submitted in partial satisfaction of the requirements for the degree Doctor of Philosophy

in

Neurosciences

by

Jason Elliott Pipkin

Committee in charge:

William B. Kristan, Jr., Chair
Edward M. Callaway
Hollis Cline
Mark H. Ellisman
Kathleen A. French
Maryann E. Martone

2015

The Dissertation of Jason Elliott Pipkin is approved, and it is acceptable in quality and form for publication on microfilm and electronically:

_____

_____

_____

_____

_____

_____
Chair

University of California, San Diego

2015

TABLE OF CONTENTS

LIST OF FIGURES AND TABLES

Chapter 2.

Chapter 3.

Chapter 4.

Appendix A.

ACKNOWLEDGEMENTS

I am indebted to Professor Bill Kristan, my advisor, for taking me in to the lab as a wayward second year and allowing me the freedom to pursue an ambitious project. It is rare in academia to find an advisor who both genuinely cares for his or her students and who has the skills to know when to nudge them along in a different direction and when to stand aside and let them work. In this, Bill's advising has been exemplary. The lab atmosphere he and Professor Kathy French engender is a rare mix of scientific intensity and authentic warmth and openness. On this note I would also acknowledge Joyce Murphy, the lab manager who maintains our leech colony and lab solutions and without whom none of the work in this thesis would have been possible. I would also thank the many labmates I've known while in the Kristan lab for being a resource for both information and conversation. These include Krista Todd, Paxon Frady, Benjamin Migliori, Chris Palmer, and the many undergraduate and master's students who worked in the lab during my time here.

I would like to strongly acknowledge the contribution of Professor Mark Ellisman and his staff at NCMIR, including Eric Bushong, Tom Deerinck, Mason Mackey, and others, for their invaluable and necessary collaboration in my thesis work. It is impossible to do electron microscopy without electron microscopes, and Professor Ellisman was very generous with allowing me access to their state-of-the-art equipment, staff, reagents, and data storage. I would particularly thank Eric Bushong for his patient and calm assistance with sample preparation and imaging.

Finally, I would thank the leeches, whose beautiful nervous system is the reason this thesis exists in the first place.

Chapters 2 and 3 represent work being prepared for publication. Jason Pipkin, Eric Bushong, Mark Ellisman, William Kristan. The dissertation author was the primary investigator and author of this material.

VITA

2009	Bachelor of Arts, Carleton College
2015	Doctor of Philosophy, University of California, San Diego

ABSTRACT OF THE DISSERTATION

Untangling the Ganglion: Connectomics in the Medicinal Leech

by

Jason Elliott Pipkin

Doctor of Philosophy in Neurosciences

University of California, San Diego, 2015

Professor William B. Kristan, Jr., Chair

The behaviors generated by neural circuits are constrained by the connectivity pattern among the neurons involved. Determining this connectivity pattern for circuits involving more than a handful of neurons becomes infeasible for physiological approaches that measure how the membrane potential of one neuron is affected by currents elicited in another. On the other hand, determining connectivity by anatomically discovering synapses is difficult due to the complicated and intertwining arbors that neurons possess. One approach to unravel this knotty problem is to image serial thin sections of neural tissue with

an electron microscope. In this thesis, I describe the first application of large scale serial electron microscopy to the ganglion of the medicinal leech, *Hirudo verbana*. The leech ganglion is an ideal preparation for this experiment as it is compact enough in size that it is feasible to collect images spanning an entire ganglion. Here, I discuss results we collected from two image volumes of leech tissue. One spans a small region of adult ganglion neuropil, while the other includes an entire ganglion belonging to a juvenile leech. In these volumes, I reconstruct three-dimensional representations of neuronal arbors and locate the synapses between them. In Chapter 2, I show that we can differentiate neurons on the basis of where synaptic input and output sites are distributed throughout their arbors. In Chapter 3, I show that we can locate the synapses between pairs of neurons previously known to be connected, and that we can discover new synapses anatomically that are then recovered physiologically. Together, these results demonstrate the potential that this "connectomics" approach has when applied to the already physiologically accessible leech ganglion.

Chapter 1. Introduction.

Across phylogeny, animals' nervous systems serve to detect salient features of their internal and external environments, process the resulting information, and decide and coordinate a behavioral response. Within nervous systems, the interactions of electrically excitable cells known as neurons at specialized sites called synapses enable this transfer and alteration of information (Sherrington, 1906). Groups of synaptically-linked neurons form circuits whose functions are circumscribed by the physiological properties of the neurons involved, the influence of molecules which modulate those properties, and especially by the pattern of synaptic connectivity within the circuit.

Research into circuit function thus necessitates understanding how the neurons involved are connected to each other. There are two basic approaches to studying synapses: through physiology or anatomy. Experimentally, physiological approaches entail inducing electrical activity in one neuron (the presynaptic neuron) while recording whether and how a second neuron's electrical activity is altered (the postsynaptic neuron). Anatomical study instead seeks to identify the physical location where a process of the presynaptic neuron forms a presynaptic bouton full of vesicles and, apposed to this bouton across a very narrow gap (the synaptic cleft), lies a process of the postsynaptic cell.

Visualizing synapses anatomically is complicated by the gross organization of many nervous systems into "neuropils" in which the tangled processes of many neurons intertwine and mingle (Apathy, 1905). Therefore in order to detect a synapse between two neurons it is necessary to have some means of selectively visualizing only the branches of those two neurons. This is achieved by staining or labeling the neurons with an indicator visible under the light microscope. Historically, techniques to selectively label neurons have ranged from

Golgi's stain (Golgi, 1873), filling neurons with fluorescent dye (e.g. Maranto, 1982), or inducing the expression of fluorescent proteins like GFP (Chalfie et al., 1994). Synaptic structures themselves can be labeled in this way. For example, it is possible to label proteins specialized to presynaptic structures in one cell with one color of a fluorescent marker and label postsynaptic proteins in the other cell with a fluorescent marker of a different color (e.g. Dani et al., 2010). It is also possible, in mammalian nervous systems, to use engineer the genetic cargo of viruses like Rabies that naturally travel from one cell to its presynaptic partners with fluorescent makers and determine synaptic connectivity in this way (Wickersham et al., 2007).

There are some major limitations to the scalability of these approaches. A given circuit of interest can involve tens to hundreds to thousands of neurons whose processes all interact within the same region of neuropil. Even a technique invented to label every neuron with a different color (generating a so-called "Brainbow") fails to adequately enable the precise tracking of thin neuronal processes in such dense regions (Livet et al., 2007). And if this technique could be refined it would still need to be paired with a means to label pre- and postsynaptic structures.

Electron microscopy (EM) addresses the resolution problem of light microscopy. With an electron microscope, it is possible to resolve the presynaptic vesicles, the synaptic cleft, and the postsynaptic process (e.g. Gray, 1959). For this reason, EM is considered the "gold standard" for synapse identification. Of course, the same labeling problems persist – in order to test a particular synapse, one needs to be able to determine that the presynaptic bouton and postsynaptic process in question belong to the hypothesized neurons. This can

also be achieved by filling neurons with electron dense material (e.g. Wadepuhl, 1990) or even genetic labeling (Deerinck et al., 2013; Atasoy et al., 2014; Lam et al., 2015).

In theory, the ability to methodically analyze several serial EM images taken of a large enough region of neuropil should enable a researcher to catalogue the shape and synapses of every neuronal arbor in that region. In such a way it would be possible to generate a map of connectivity of every neuron identifiable and traceable in the volume of EM images. Sydney Brenner's group was the first to apply the potential of EM for revealing neuronal circuitry by imaging and analyzing an entire individual of the nematode species *C. elegans* (White et al., 1986). This effort revealed every connection among all 302 neurons of this organism, enabling insight into the individual and collective ways these neurons participate in the behaviors of the animal. Such comprehensive maps of connectivity are today referred to as "connectomes" (first usage by Sporns et al., 2005).

Generating connectomes from serial EM images is a difficult and time-consuming process. The *C. elegans* connectome took over a decade to construct from a volume of images spanning only 302 neurons. Upscaling this process to tackle even a larval *Drosophila* (~10,000 neurons; Ohyama et al., 2015) seemed infeasible until very recently. In the past decades, new technologies have been developed that accelerate the pace of image acquisition. For the transmission electron microscope, these have involved techniques to enhance the reliability and speed of acquiring thin sections of tissue (serial section transmission electron microscopy, ssTEM) (Harris et al., 2006; Kasthuri et al.; 2015). For the scanning electron microscope, advances in the detection of backscattered electrons combined with in-chamber automated ultramicrotomes have similarly increased the speed of

imaging in a process called serial blockface electron microscopy (SBEM) (Denk and Horstmann, 2004).

Applications of these new imaging techniques have led to the acquisition of high resolution EM datasets in which it is possible to map the connectivity of circuits of interest contained within the imaged volume. Subsequently, it has been applied to the study of circuits in the mouse retina (Briggman et al., 2011; Helmstaedter et al., 2013) and cortex (Bock et al., 2011; Kasthuri et al.; 2015), the *Drosophila* larva (Ohyama et al., 2015), and the tail of the male *C. elegans* (Jarrell et al., 2012). The visual system of invertebrates has received quite a bit of attention as well, with serial EM studies on the copepod (Lacalli, 2009), the fruit fly (Takemura et al., 2013), the pycnogonid (Lehman et al., 2014), and the flatworm (Randel et al., 2014; Randel et al., 2015). In addition to connectivity, a trove of information on neuronal structure is present within serial EM datasets, and this has been used to inform a range of questions from the study of the diversity of synaptic arrangements in the hippocampus (Wilke et al., 2013), to modeling the diffusion of molecules through extracellular space in neuropil (Kinney et al., 2013), and to the study of the structure of hippocampal synapses in an Alzheimer's disease mouse model (Wilke et al., 2014).

The acquisition of serial EM datasets spanning large volumes of tissue has the potential to reveal structure and connectivity at an unprecedented scale. In this thesis, I describe the application of SBEM on tissue belonging to the nervous system of the medicinal leech, *Hirudo verbana*. The medicinal leech has been a favored system for the physiological study of circuit function. The nervous system of the leech comprises 32 ganglia arrayed along the ventral length of the animal and linked by three nerve connectives. Each ganglion defines a segment of the annelid leech. The 21 segments of the midbody of the leech are

each served by a homologous ganglion containing nearly the same number and complement of neurons. Because of this homology, it is possible to reliably study the same circuitry from ganglion to ganglion and animal to animal. Within a ganglion, the exterior comprises a layer of ~400 large neuronal somata who each extend a single process into a central region of neuropil that subsequently branches profusely and synapses with other neuronal arbors. The size and external arrangement of the somata renders the ganglion particularly accessible to electrophysiological and optical techniques.

In addition to its physiological amenability, the ganglion is also well-suited to complementary anatomical exploration via serial EM. In Chapter 2, I present a manuscript in preparation characterizing the composition and spatial patterns of synaptic structures within various arbors reconstructed from both a small volume of neuropil acquired from an adult leech and from a volume spanning an entire ganglion from a juvenile leech. In Chapter 3, I present a manuscript in preparation discussing the synaptic connections revealed in the juvenile ganglion dataset. Together, these works demonstrate the utility and potential of the leech nervous system for future connectomic analysis.

As this work involves the application of relatively new techniques, I thought it useful to include brief discussions of the various challenges that one encounters in generating and analyzing these datasets. These are available in Appendix A (Parameters and challenges of data acquisition) and Appendix B (Challenges in analysis of large volumes of serial EM data).

Chapter 2. Patterns and distribution of presynaptic and postsynaptic elements within leech neuronal arbors.

Abstract:

The exterior layer of the ganglion of the leech nervous system contains ~400 neurons whose profusely branching arbors synapse with each other and with arbors arising from neurons in neighboring ganglia in a central region of neuropil. Cataloguing the diversity of ultrastructural features in the neuropil has heretofore been limited to analysis of single sections or short image series, precluding the ability to discern how synaptic features like vesicles and postsynaptic input sites are distributed in three dimensions throughout a given neuron's arbor. We applied serial blockface electron microscopy (SBEM) to two samples of leech tissue. In the first, a small volume of neuropil from an adult ganglion, we characterize the distribution of synaptic vesicles and find that individual arbors tend to have the same complement of vesicles throughout. We also observe a small fraction of arbors which lack vesicles altogether. In the second sample, we image an entire ganglion from a juvenile leech and use the resulting data to link vesicle phenotype to known cells and to reveal that some neurons segregate their arbors into input-only zones and mixed input and output zones while other neuronal arbors contain only a mixed input and output zone. These results represent the first detailed three-dimensional reconstructions of neurons in the leech and underscore the potential of SBEM for revealing previously unknown features of synaptic input and output distribution.

Introduction

The nervous system of the medicinal leech (*Hirudo verbana*) is composed of a chain of homologous ganglia linked by three connective fascicles. Each ganglion comprises an outer layer of large neuronal somata (20-70 μm in diameter) who extend their primary process into an inner region of dense neuropil. Within the neuropil, neurons form profusely branched arbors that span large areas and synapse with other arbors (e.g. Muller and McMahan, 1976; DeRiemer and Macagno, 1981; Fan et al., 2005).

The outer layer of somata has been well-characterized ultrastructurally (Cray and Guillery, 1963; Coggeshall and Fawcett, 1964). All the neurons feature a central nucleus surrounded by numerous mitochondria and an elaborate network of endoplasmic reticulum which spans the entirety of the cytoplasm. A few somata contain numerous dense-core vesicles while most do not (Coggeshall and Fawcett, 1964). In at least two neurons, these vesicles can be released directly from the somata (Trueta et al., 2012). All the intracellular features of the somata are bounded by a plasma membrane that is frequently invaginated by processes of glial cells that reside amongst the neurons (Cray and Guillery, 1963; Coggeshall and Fawcett, 1964).

To date, ultrastructural interrogation of the leech neuropil has been limited to what can be observed in single sections or a limited number of serial sections. Muller and McMahan (1976) used serial section transmission electron microscopy (ssTEM) to describe the general structural arrangement leech synapses as comprising a large presynaptic varicosity apposed by several indenting postsynaptic processes. In order to link neuropilar structure and synapses to known cells, past efforts have employed chemical labeling approaches (e.g. somatic injection with horseradish peroxidase that is subsequently reacted

with diaminobenzidine to form an osmiophilic product) that render the cytoplasm of that cell's processes differentiable from others (Muller and McMahan, 1976; Muller and Carbonetto, 1979; Granzow et al., 1985; Wadepuhl et al., 1990). While useful for many applications, these stains also tend to obscure and occasionally disrupt intracellular structures like synaptic vesicles (Granzow et al., 1985).

The aim of the present study was to extend these efforts beyond single and small series of thin sections in order to reveal the organization and distribution of synaptically involved areas in neuronal arbors. We employed serial blockface scanning electron microscopy (SBEM) to generate two large volumes of leech neuropil. The first contains a portion of neuropil from an adult ganglion which we used to describe patterns of vesicle distribution and synaptic arrangements in mature leech tissue. The second contains an entire ganglion (somata and neuropil) from a juvenile leech. We selected the smaller juvenile leech for practical purposes: their smaller ganglia (~60% the diameter of an adult's) enable a reasonable imaging time (in our case, six weeks). Importantly, juveniles perform many of the same behaviors studied in the adult: they swim, crawl, shorten, bend, and feed (though they do not participate in reproductive behaviors). We use the juvenile ganglion dataset to link patterns of synaptic arrangements to known cells and to report the distribution of synaptic inputs and outputs in single cells throughout the entirety of the ganglion-contained portion of their arbors.

Materials and Methods

Animals

We used both adult and juvenile medicinal leeches, *Hirudo verbana.* Adult leeches were obtained from Niagara Leeches (Niagara Falls, NY) and housed in aquaria on 12 h daily light/dark cycle at 15-16°C. Juvenile leeches were obtained by harvesting cocoons produced by a breeding colony of adult leeches maintained in our laboratory. Leeches were allowed to mature within the cocoons at RT and collected once they had emerged. We then waited two weeks to ensure full development prior to dissection. We confirmed that the juveniles lacked any embryonic features using established staging criteria (Reynolds et al., 1998).

Sample preparation

Both adult and juvenile samples were prepared with the same protocol. We anesthetized the leeches in ice-cold leech saline (4°C) containing 115mM NaCl, 4 mM KCl, 1.8mM $CaCl_2$, 2mM $MgCl_2$, 10mM HEPES buffer (Nicholls and Purves, 1970). Midbody ganglia were then dissected from the nerve cord and pinned them to the bottom of Sylgard-coated dish. The ganglia were then fixed for two hours RT in 2% PFA, 2.5% glutaraldehyde, and .1M phosphate buffer. After that the ganglia were rinsed in .1M phosphate buffer and incubated in 2% OsO_4 / 1.5% potassium ferrocyanide. For this step, the samples were microwaved in a scientific microwave three times with a duty cycle of 40s on and 40s off at a measured temperature of 35°C and subsequently left to sit at RT for thirty minutes. Samples were then washed in ddH_2O and microwaved three times with a 2 minutes on and 2 minutes off duty cycle at 30°C. We found that this and subsequent brief microwave incubations facilitated staining penetration to the center of our samples and was necessary to gain sufficient image contrast. Samples were then incubated in 1% thiocarbohydrazide (EMS) and microwaved

three times with a 40s on and 40s off duty cycle at 30°C and subsequently left to incubate for 15 minutes RT. The samples were then washed again with the same microwave incubation as described earlier. Next, the samples were incubated in 2% aqueous OsO_4 and microwaved three times with a 40s on and 40s off duty cycle at 30°C and then incubated at RT for one hour. After washing, the samples were then left in 1% uranyl acetate overnight at 4°C. The next day, samples were incubated in a lead aspartate solution prepared by dissolving 0.066gm of lead nitrate into 10ml of 0.003M aspartic acid with the pH subsequently adjusted to 5.5 using 1N KOH. This incubation took place in a 60°C oven for 30 minutes. Next, the samples were washed and dehydrated through a series of ethanol solutions (50%, 70%, 90%, 100%, 100%, 10 minutes each) at RT and finally incubated in acetone. Next, samples were infiltrated with plastic by first incubating them for two hours at RT in a solution of 50% acetone and 50% Durcupan and then overnight in 100% Durcupan. The next day, samples were transferred to a freshly prepared 100% Durcupan solution and incubated at RT for 2 hours. Samples were then incubated within a 60°C oven for three days. Durcupan Araldite resin was made by mixing 11.4g of component A, 10g of component B, 0.3g of component C, and 0.1g of component D.

Imaging

The plastic-embedded ganglia were preserved within carefully-trimmed plastic blocks. For transmission electron microscopy, thin sections were cut and mounted on copper grids (no additional staining was performed) and subsequently imaged with a JEOL 1200 TEM. For scanning electron microscopy, blocks were trimmed until tissue was barely exposed. For the juvenile sample, the edges of the block were trimmed until very near to the external capsule of the ganglion in order to reduce charging in the outer image tiles that

would contain both tissue and empty plastic. Blocks were mounted onto pins to which they were adhered with conductive silver paint. The pin and block were then sputter coated with a thin layer of gold and palladium to further enhance conductivity.

We imaged two samples. The first sample of adult ganglion neuropil was acquired at high vacuum on an FEI Quanta FEG SEM equipped with a Gatan 3VIEW SBEM system. The accelerating voltage was 2.5 kV with a dwell time of 8µs over an 8000 x 8000 pixel raster. Each square pixel measured 11.7 nm on a side and 276 sections were cut with a thickness of 70nm, resulting in a total imaged volume of 96µm x 96µm x 17.3µm. The second sample of the entire juvenile ganglion was imaged on a Zeiss MERLIN SEM equipped with a GATAN 3VIEW SBEM system. We collected montages of 8000x8000 raster tiles at 5.7nm pizel size. We oriented the sample so that it was imaged from the dorsal surface to the ventral surface with sectioning occurring perpendicular to the dorsal-ventral axis. Montage size thus varied from 1x1 to 5x5 tiles depending on how large the area of tissue was that was exposed to the surface of the block. We sectioned the block 2203 times at 50, 100, or 150 nm thicknesses for a total z-distance of 138µm. The 100nm and 150nm sections were taken in regions containing only cell bodies (at the top and bottom of the overall volume) as there were no fine neuronal processes to trace here and thus imaging time could be reduced. Similarly, we varied dwell time throughout acquisition along a range of 0.8µs to 1.5µs with higher dwell times used in neuropil-containing sections. During the juvenile ganglion acquisition, an unexpected and gradual reduction of contrast gradually occurred due to an unexpectedly early degradation of the filament in the electron gun. As imaging proceeded from the dorsal surface towards the ventral, we therefore focused most of our analysis and reconstruction on cells whose arbors tended to fall within the dorsal half of the ganglion.

Reconstruction

For the adult ganglion, images were aligned, analyzed, and visualized using IMOD (Kremer et al., 1996; http:/bio3d.colorado.edu/imod/). In this dataset, we traced the full neuronal membrane of target arbors in each section and separately recorded the location of features of interest, including synapses. We fully segmented 96 arbors within this volume. In the juvenile ganglion volume, montages and sections were aligned in the TrakEM2 (Cardona et al., 2012). Subsequent tracing and annotation was also performed in TrakEM2. In this volume we largely traced arbors via skeletonization rather than full segmentation of everything within a given neurons plasma membrane.

All tracing, segmentation, and analysis was performed by JP. In order to reduce errors, the arbors of the motor neurons discussed in Table 1 and Figures 10 and 11 were reviewed at least twice. As has been previously reported we found that false negatives (missing branches) were far more likely errors than false positives (adding the wrong branch) (Ohyama et al., 2015).

Results

Adult Neuropil

To study basic structural patterns of synaptic connectivity and describe the anatomy of the leech neuropil, we first collected a 96µm x 96µm x 17.3µm volume (about 5% of the total neuropil) from an adult ganglion. When we reconstructed neuronal arbors in this volume we found that most were both presynaptic and postsynaptic to other arbors. Some arbors however, contained no aggregations of presynaptic vesicles and were only postsynaptic to other arbors. Note that these observations are confined only to chemical synapses as gap junctions cannot be positively identified at SBEM resolution. We sampled the volume at random points, visually inspecting the arbor that contained each point. When doing so, we found that in this volume 87% (131/151) of neuronal arbors contained vesicles and the remaining 13% (20/151) did not.

The arbors which lacked vesicles branched profusely and received synaptic input from the presynaptic boutons of many other arbors. With our SBEM staining protocol, these arbors tended to have distinctly clear cytoplasm, making them stand out in higher contrast from the surrounding neuropil (Figure 1A). We reconstructed several of these vesicle-lacking arbors, revealing their profuse branching patterns (three of which are shown in Figure 1B,C). Among the three arbors shown here, there is some diversity in the thickness of major branches and number of small branches. Note that all contain numerous short and thin (<250nm diameter) branches (Figure 1C); these we found often terminated in apposition to presynaptic boutons and varicosities of other arbors (see arrowhead, Figure 1A).

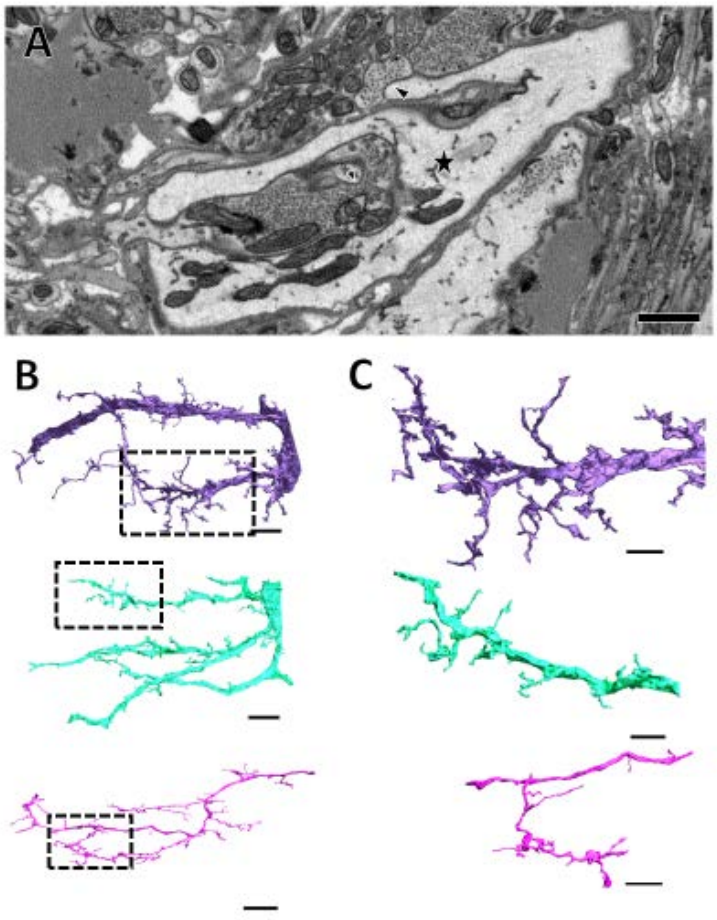

Figure 1. **Vesicle-lacking arbors. (A)** A single section of a vesicle-lacking arbor, denoted by the star symbol. A branch can be seen extending from the top of the arbor where it terminates apposed to a presynaptic bouton (arrowhead). 1000nm scale bar. **(B)** Three vesicle-lacking arbors are shown reconstructed in 3D. The arbor shown in A is the purple arbor here. 10µm scale bars. **(C)** Closer views of the boxed regions in (B) reveal the fine structure of small processes. 5µm scale bars.

We defined a presynaptic bouton as a region of an arbor in which there was an aggregation of small synaptic vesicles (Figures 2-4) with a maximal diameter of 40 nm (because our cutting thickness was too coarse to reliably estimate the size of the vesicles, we instead measured maximal diameters). In some vesicle-containing arbors, small synaptic vesicles are the only kind of vesicle present, though in other boutons they were accompanied

by scattered larger vesicles that typically reside near the edges of the synaptic vesicle field (Figure 2C,D,E). In other arbors, these fields of small vesicles were surrounded by numerous larger vesicles (Figures 5 and 6).

The most frequently observed synaptic arrangement consisted of a single presynaptic bouton closely apposed to several smaller clear postsynaptic processes (Figure 2). Because postsynaptic densities are not observed in conventionally-stained leech tissue (refs: Coggehsall et al., 1964; Muller and McMahan, 1976; Muller and Scott 1981), we developed criteria for synapse identification in our SBEM and TEM images. In TEM, we found docked vesicles at sites where the presynaptic membrane closely followed the conformation of the postsynaptic arbors (Figure 2A); we detected this same pattern in the lower resolution SBEM sections (Fig. 2B). Our major criterion for identifying chemical synaptic sites, therefore, was a concentration of vesicles in the presynaptic cell, some of which were close to membrane appositions of the pre- and postsynaptic cell (Figure 2B). In addition, in SBEM, we found that the apposition of membranes typically persists for three or more consecutive sections and often included an indentation of the presynaptic membrane into which the postsynaptic cell protrudes (Figure 2A, B). When we analyzed the synapses made by a random sample of 58 presynaptic boutons, we found that 42% (152/360) of the postsynaptic processes were at least slightly indented into the presynaptic bouton. This overall pattern also matches what has been previously established to identify leech synapses in ssTEM (Muller and McMahan, 1976; Muller 1979).

When reconstructed in three dimensions, the presynaptic boutons appeared as enlarged varicosities linked by thinner processes (Figure 2E). Each bouton had a large volume of small synaptic vesicles whose proximity to the presynaptic membrane defined a

synaptic site (dark blue membrane, Figure 2C-E). Typically, apposed to this region were several postsynaptic processes (one of which is reconstructed in pink, Figure 2C-E). Notably, we often found that arbors that were postsynaptic to one bouton of a presynaptic neuron were also postsynaptic to other boutons of that same neuron (Figure 2E). The pink postsynaptic arbor shown in Figure 2E is the same as the vesicle-lacking arbor shown in Figure 1B,C.

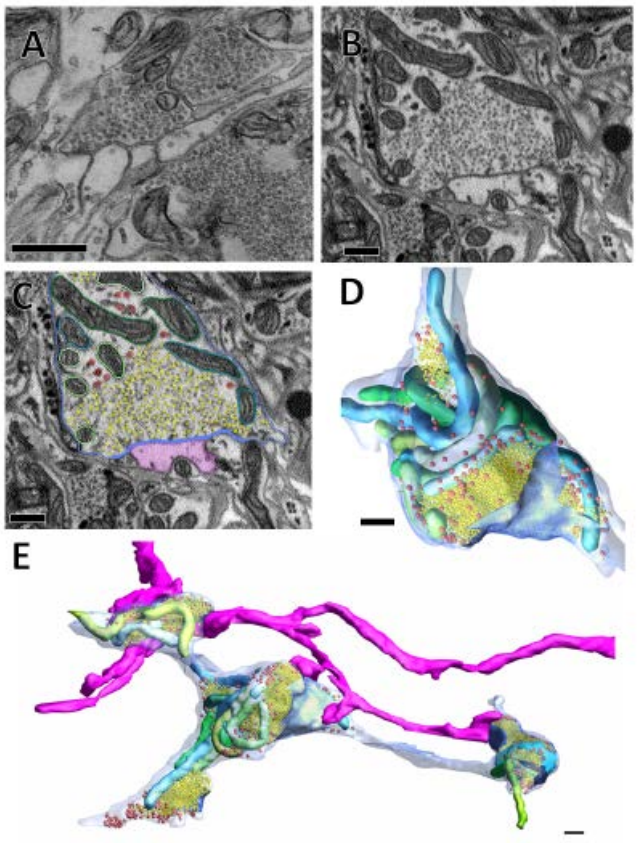

Figure 2. **Typical synaptic arrangements**. In TEM and SBEM these involve a vesicle-filled bouton apposed to several smaller postsynaptic processes. **(A)** A thin section imaged with TEM showing the indenting apposition of numerous postsynaptic processes to a single presynaptic process with some docked vesicles visible. **(B)** A similar arrangement now observed in SBEM. **(C)** The same image in B now segmented so that the plasma membrane is blue; the region of plasma membrane in close proximity to synaptic vesicles is darker blue; synaptic vesicles are yellow; scattered larger vesicles are red; mitochondria are individually segmented in various shades of blue and green; a postsynaptic process (same as in Figure 1B,C) is shown in pink. **(D,E)** The three dimensional reconstruction of the bouton and its neighbors along with the postsynaptic process. 500nm scale bars in all panels.

Vesicle fields varied considerably in size, even in two boutons on a single arbor (Figure 3). Nearly all vesicle fields had several mitochondria nearby (Fig. 3A) with the exception of some smaller vesicle fields (Figure 3B), even when examined in three dimensions. Although most arbors contained vesicle fields only within thinner (<1 µm in diameter) secondary branches, some primary branches had vesicle fields as well, often at branching sites (Figure 3C).

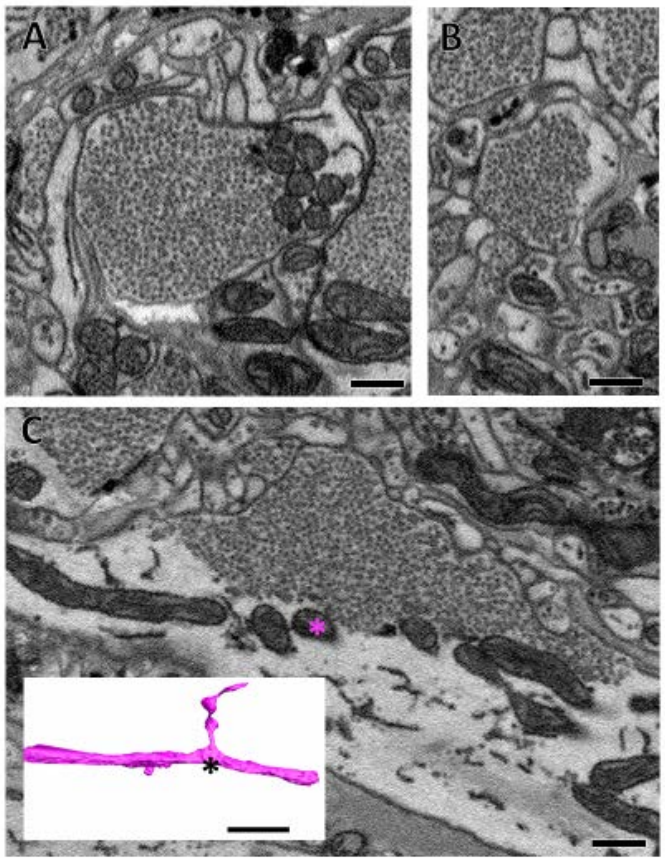

Figure 3. **Variable vesicle field size**. **(A-C)** Individual boutons of a single arbor containing varying sizes of vesicle fields. In (C), the vesicle field is located at a branching site in the overall arbor, depicted in the inset. Scale bars 500nm (A-C), inset in (C) has 10µm scale bar.

Generally, most arbors contained vesicle fields that were densely packed within a bouton along with mitochondria and other structures (Figures 2, 3, 7). In some arbors, however, vesicle fields inhabited relatively small regions within a process (Figure 4). In these arbors we frequently observed two or more vesicle fields in a single section (arrows, Figure 4).

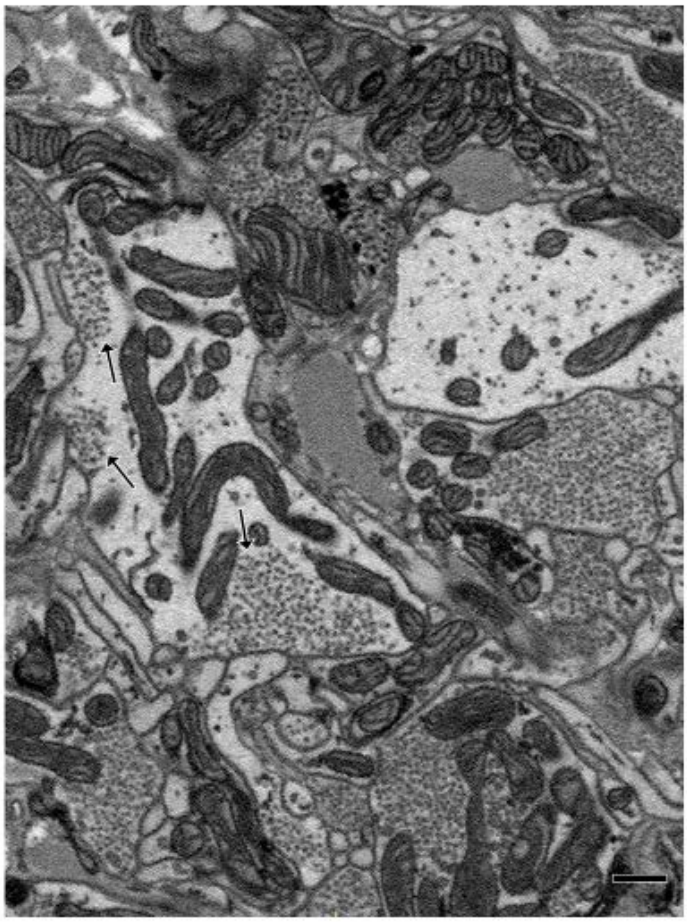

Figure 4. **Non-filling vesicle fields.** Some arbors contained vesicle fields which did not fill the entire process within which they were contained. In these arbors it was common to observe multiple vesicle fields in the same section (arrows). Scale bar 500nm.

Presynaptic boutons are linked together by thinner inter-bouton processes (Figure 2E). In some cases we could trace back from a presynaptic bouton to the point where the

small branch split off from the large primary process of the neuron (due to the small size of this volume, many arbors did not contain their primary branch). These primary processes are typically devoid of the small synaptic vesicles (Figure 5A), though some do contain presynaptic vesicle fields (Figure 3C). We also observed one primary branch that contained several small vesicle fields that did not appear to be involved in any synaptic activity, given the lack of any apposed postsynaptic arbors in their vicinity (Figure 5B). In this case, the secondary branches of this cell formed presynaptic arrangements comprising several relatively small vesicle fields similar to those documented in Figure 4.

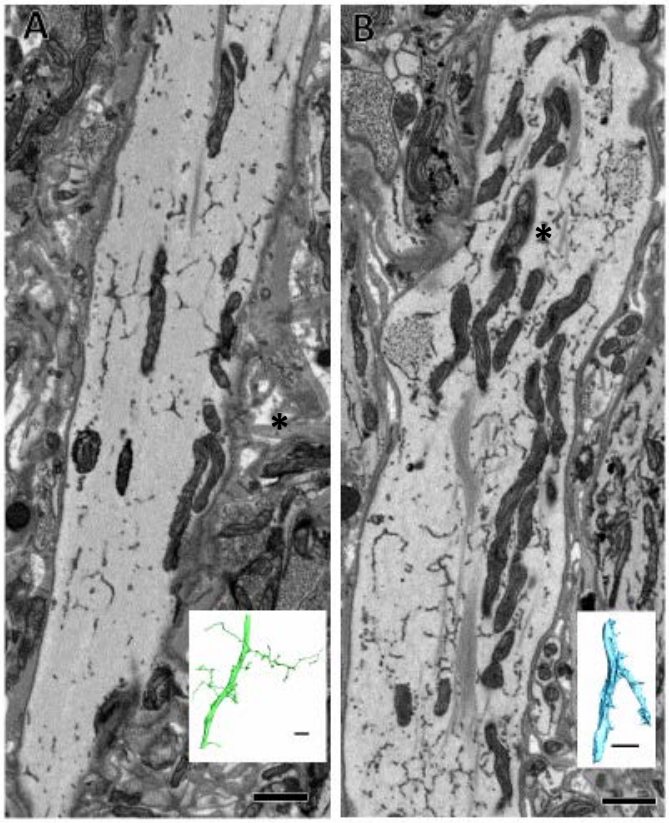

Figure 5. **Primary process vesicle content.** Primary processes belonging to vesicle-containing arbors may or may not contain vesicles. **(A)** A cross section of a primary process belonging to a vesicle-containing arbor shown in green in inset. No vesicles are present. **(B)** Another primary process belonging to a vesicle-containing arbor in which clusters of vesicles are visible (asterisks) yet are not presynaptic to any other arbor. Inset shows the full reconstruction of this arbor. Scale bars 1000nm for micrographs, 10µm in insets.

As noted previously, some arbors contained a population of larger vesicles. These larger vesicles are often found surrounding fields of small presynaptic vesicles, though we also found them in relative isolation, scattered throughout the containing arbor. We broadly divided the arbors containing these larger vesicles into two categories on the basis of how intensely the vesicles stained.

We found some arbors that contained intensely dark-stained vesicles 100 nm in maximal diameter (Figure 6). If the arbor contained presynaptic boutons, these vesicles were found in aggregations adjacent to--and partially overlapping with—the fields of small vesicles (Figure 6A, B). In general, presynaptic boutons of this arbor type were smaller and contained smaller vesicle fields (see Figure 9). Aggregations of the larger intensely-stained vesicles were also occasionally encountered in the absence of any immediately-adjacent small vesicle fields. In between presynaptic boutons, these arbors contained scattered individual large vesicles (Figure 6C, D). We also found one arbor that contained the intensely dark stained vesicles scattered within primary branches and throughout all of its secondary branches, even though the arbor lacked any boutons containing fields of small vesicles (Figure 6E).

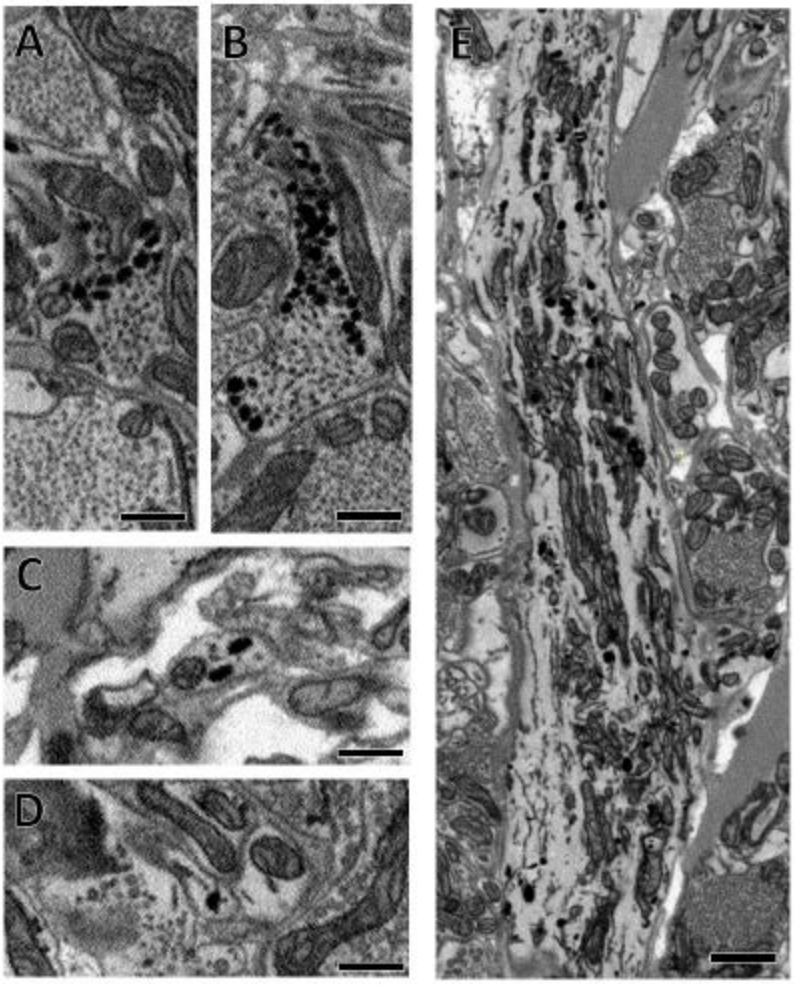

Figure 6. **Intensely-staining dark vesicles**. **(A,B)** Examples of aggregations of these large dark vesicles surrounding fields of presynaptic vesicles. **(C,D)** These large vesicles were found scattered throughout the thin processes which interlinked presynaptic boutons. **(E)** The primary process of one arbor which contains many scattered large dark vesicles. This particular arbor never formed any presynaptic boutons in the volume. (A-D) scale bars 500nm, (E) scale bar 1000nm.

We also found arbors that contained a population of large (100 to 170 nm in maximal diameter), close-packed vesicles. Unlike the darkly staining vesicles, the maximal diameters of these vesicles were larger and more lightly stained, ranging from grey to clear (Figure 7A-C). These large, lightly staining vesicles were sometimes associated with much larger

presynaptic boutons (Figure 7C). Aggregations of these large vesicles can be found independently of small vesicles and scattered in the thin processes connecting presynaptic boutons (arrowheads, Figure 7B). Occasionally scattered glycogen particles are observed interspersed among these very large vesicles (Figure 7C), a pattern also observed by earlier researchers (Coggeshall and Fawcett, 1964). Similar to the arbor shown in Figure 6E, we also found one arbor that contained large, clear vesicles scattered throughout its primary and secondary branches, despite not containing any fields of small vesicles (data not shown).

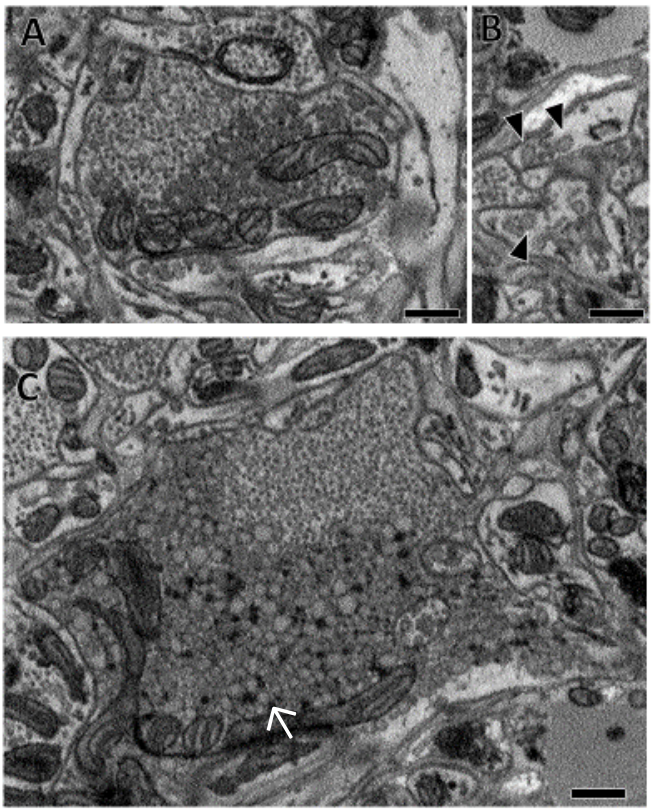

Figure 7. **Very large clear vesicles.** Some arbors contained very large vesicles (170nm maximal diameter) ranging in coloration from dark to light grey. **(A)** An example bouton with a population of small synaptic vesicles surrounded by an aggregation of large dark grey vesicles. **(B)** Similar to the very dark vesicles depicted in Figure 6 C-D, these large lighter staining vesicles were seen in the thin processes between boutons (arrowheads). **(C)** Some boutons containing these large vesicles were very large. Dark glycogen particles are scattered throughout these large vesicles (arrows). Scale bars 500nm.

We were interested in how frequently we observed arbors that contained either the intensely-stained dark vesicles or the large clearer vesicles. As noted above, we conducted an analysis where we visually inspected the arbor containing a randomly generated point in the volume. Of the vesicle-containing arbors, 70% (92/131) did not contain aggregations of either large clearer vesicles or large intensely-stained dark vesicles (though some of these did contain scattered larger vesicles as in Figure 2). Four percent (5/131) contained intensely stained dark vesicles and the remaining 26% (34/131) contained aggregations of either grey (Figure 7A) or clear (Figure 7C) vesicles.

We next asked whether the vesicle content of a given bouton influenced the number of postsynaptic partners it had. For this analysis, we outlined the fields of presynaptic vesicles at 59 boutons each taken from the set of arbors we analyzed in our random point analysis. In addition, we included more samples of selected boutons containing intensely-stained dark vesicles and large clearer vesicles. We then measured the cumulative imaged area of the vesicle fields. This measure excludes any attempt at determining vesicle field volume which would require making assumptions about the distribution of vesicles in non-imaged inter-slice regions. We then plotted the cumulative imaged area of the synaptic vesicle fields versus the number of postsynaptic contacts (Figure 8). Different sized and colored circles indicate whether the bouton contained primarily small synaptic vesicles (small grey dots), intensely stained dark vesicles in addition to small synaptic vesicles (black dots), or larger clearer vesicles in addition to small synaptic vesicles (large open circles). We found a weak overall correlation between cumulative vesicle field area and number of postsynaptic partners ($R^2 = 0.1866$). Beyond that, we found that boutons that contained intensely-stained

dark vesicles tended to have smaller vesicle fields and have subsequently have fewer postsynaptic partners (black dots, Figure 8).

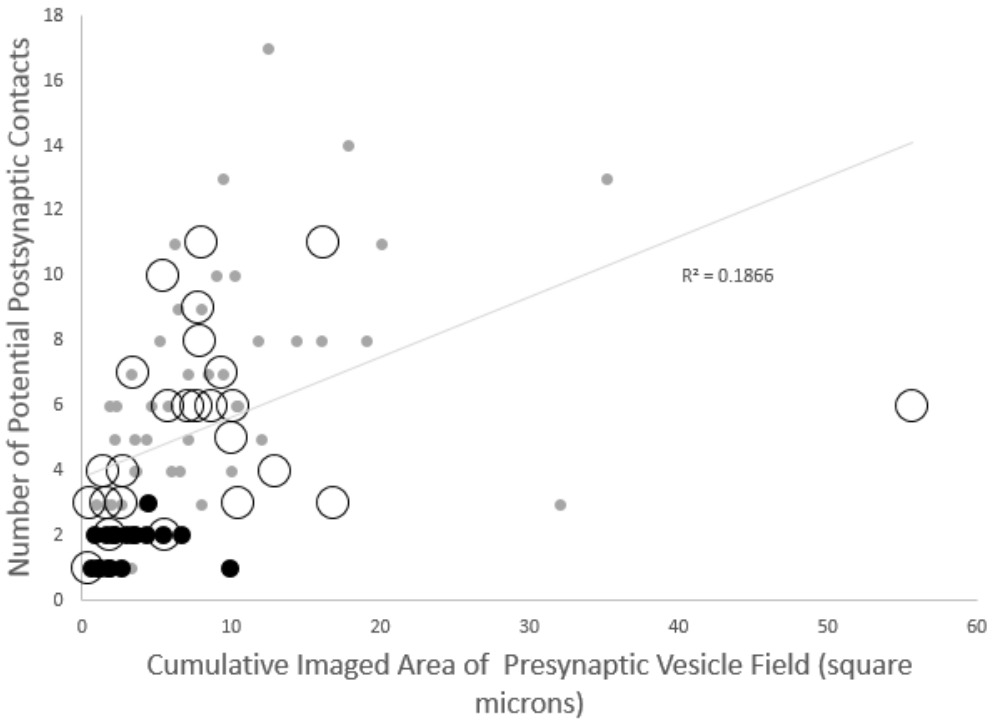

Figure 8. **Vesicle field size and postsynaptic contacts.** The relationship between the cumulative imaged area of presynaptic vesicle fields and number postsynaptic contacts at individual boutons is shown. There is an overall weak correlation between the area of vesicle fields and the number of postsynaptic contacts ($R^2 = 0.1866$); this correlation is weakened in part by the three very large vesicle fields in this dataset. Grey dots indicate that the bouton contained primarily small presynaptic vesicles; black dots indicate that the bouton contained both small presynaptic vesicles and large intensely-stained vesicles; open circles indicate that the bouton contained both small presynaptic vesicles and large clearer vesicles. At all data points only the cumulative imaged area of the small presynaptic vesicle field was calculated.

Juvenile Ganglion

After analyzing the small volume of adult neuropil, we sectioned and imaged a volume spanning an entire ganglion. To reduce acquisition time, we selected a ganglion from the juvenile leech. Juvenile leeches perform most of the same behaviors studied in the adult (Reynolds et al., 1998) yet are much smaller and possess ganglia with diameters 60% of their adult counterparts. When we performed the same random point analysis in this volume as we did in the adult, we found that 78% (115/147) of neuronal arbors contained vesicles, while the remaining 22% (32/147) did not. Compared to the adult volume, this represents a 10% increase in the fraction of arbors without vesicles.

Because the juvenile material contained the entire ganglion, we were able to map every cell body. We found 397 neurons in total: 72 in the right anterolateral packet, 71 in the left anterolateral packet, 75 in the right posterolateral packet, 78 in the left posterolateral packet, 45 in the posteromedial packet, 49 in the anteromedial packet, and 7 neurons whose somata lay just inside the inner capsule and were thus technically in the neuropil (these cells have been seen before by Coggeshall and Fawcett, 1964). Of these somata we also found a handful that contained either heavily-stained dark vesicles or the large clear vesicles (Figure 9) like the arbors described from the adult volume (Figures 6,7). Based on the locations of these cells (Figure 9C, blue cells), the cells containing the dark-staining vesicles correspond to the six serotonergic neurons, as has been previously observed (Trueta et al., 2012; Lent et al., 1991). Many of the somata containing large clear vesicles do not match any previously-identified neurons (Figure 9C, red cells), although two of these cells are clearly the Leydig cells (Figure 10B,C), based on their size and soma position.

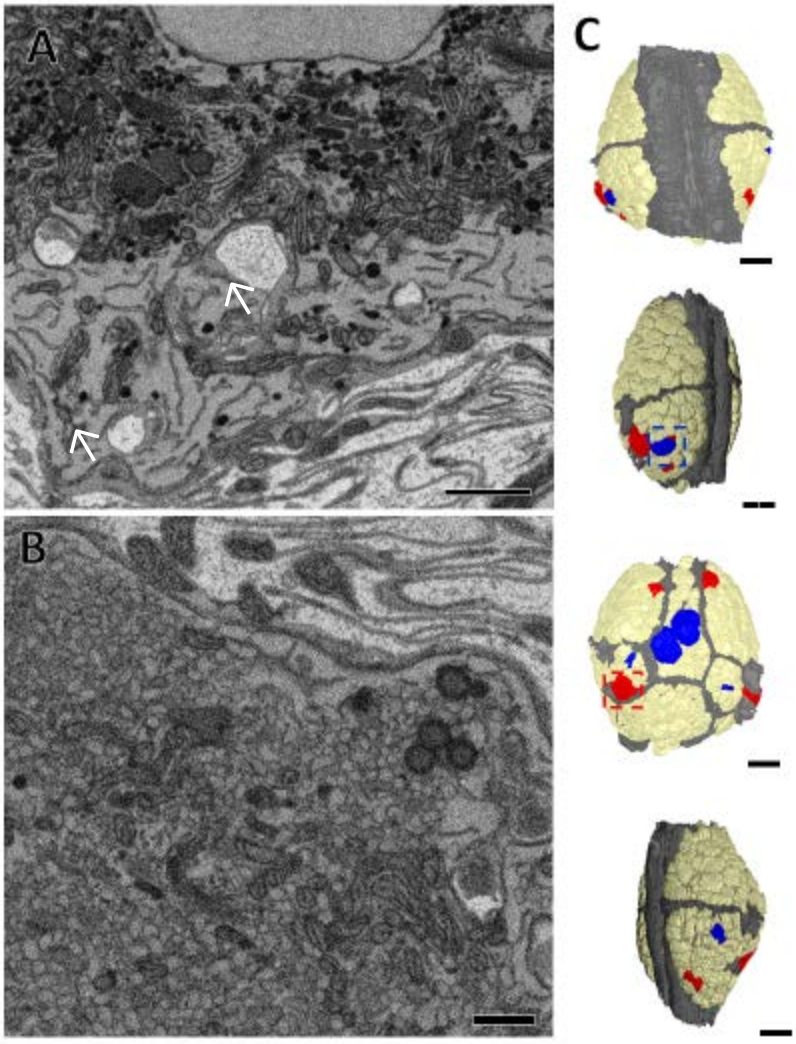

Figure 9. **Somata containing different vesicles.** The somata of some cells in the juvenile ganglion contained aggregations of intensely-stained dark vesicles or larger clear vesicles. **(A)** Image of a portion of the soma of a dark-vesicle containing cell, dark vesicles indicated by arrows. **(B)** Image of a portion of the soma of large clearer-vesicle containing cell. **(C)** Map of the ganglion with blue cells indicating the somata of neurons that contained dark vesicles, and red cells those which contained large clearer vesicles. Tan cells contained neither. Neuropilar boundary depicted in grey. Outlined in blue box is the cell shown in (A) and outlined in the red box is the cell shown in (B). Scale bars 500nm in (A) and (B), 40µm in (C).

We partially traced the arbors of some of the blue cells or red cells in Figure 9. Several of these cells extend branches into the ventral portion of the neuropil, in which thinner secondary branches are difficult to trace due to poor image quality. For those

branches which we could follow, we did not find any presynaptic specializations, though scattered vesicles were present throughout the primary and secondary branches. One pair of red cells did arborize dorsally (arrows, Figure 9C). These cells formed presynaptic boutons full of small presynaptic vesicles without any surrounding cloud of densely-packed large vesicles (despite these large clear vesicles being otherwise scattered throughout the arbor). We also attempted to backtrace from presynaptic boutons that did contain aggregations of either intensely dark-stained vesicles or larger clear vesicles in the hopes of identifying the cells to which they belonged. However, in every case we were either able not to follow the arbor all the way to a soma or we found that it belonged to an axon emanating from another ganglion that arrived via the connectives.

Because we could map every neuronal soma in the ganglion (Figure 10A), we were able to identify cells of interest which could then be traced and annotated fully. To demonstrate this, we selected the inhibitory motor neuron cell DI-1 (dorsal inhibitor 1) because many of its physiological connections have been characterized (Ort et al., 1974; Kristan et al., 2005). We reconstructed the entire arbor of the right DI-1 in the juvenile ganglion (Figure 10B). We also generated a skeleton model of DI-1 by placing a single dot within the contour of a cell's membrane in a given section of the volume (each dot, or node, is connected to the next via a line when represented graphically) (Figure 10C). Tracing arbors in this manner is common (e.g. White et al., 1986; Briggman et al., 2011; Ohyama et al., 2015) as it reduces segmentation time considerably. It should be noted however that while this skeletonizing process captures the cell's entire arbor, it does generate some false branches in thick processes that travel roughly parallel to the imaging plane. While we could have removed these by removing the nodes of these short branches, in many cases doing so

would risk leaving unlabeled a region of an arbor that contained pre- or postsynaptic zones, so we chose to leave the skeletons unedited. We then annotated this arbor by marking locations on the skeleton where we found presynaptic and postsynaptic sites, using the criteria documented in Figures 2. On the skeleton of cell DI-1, presynaptic sites were marked with red balls and postsynaptic sites with green balls (Figure 10C). The total number of input and output sites are summarized for the cells we traced and fully annotated (Table 1). The total number of synaptic inputs to the right DI-1 shown is 912 (Table 1). However, presynaptic boutons can synapse onto multiple postsynaptic partners (Figure 2) and can vary greatly in size (Figure 3). The reconstructed cell DI-1 had 261 presynaptic boutons, each of which had multiple postsynaptic targets (a range of 1 to 21, with a median and mode of 7) for a total of 1684 potential postsynaptic processes.

Table 1. **List of nodes, inputs and outputs per cell**. Vesicle-containing nodes are sites of synaptic output while synaptic input nodes are sites of input. Only one node at a presynaptic bouton was marked as "vesicle-containing".

Cell Name	Total Nodes	Vesicle-containing Nodes	Synaptic Input Nodes
S Cell	13802	232	374
Left Coupling Cell	17298	26	837
Right Coupling Cell	8659	28	428
Right DI-102	18978	95	361
Left DI-102	22669	101	511
Right 116	27507	76	415
Left 116	22787	63	286
Left VE-4	20363	0	610
Right VE-4	15202	0	321
Left DI-1	29590	90	577
Right DI-1	39928	261	912
Left VI-2	16092	59	370
Right VI-2	17191	74	402
Right DE-3	21608	6	650
Left DE-3	20161	1	437

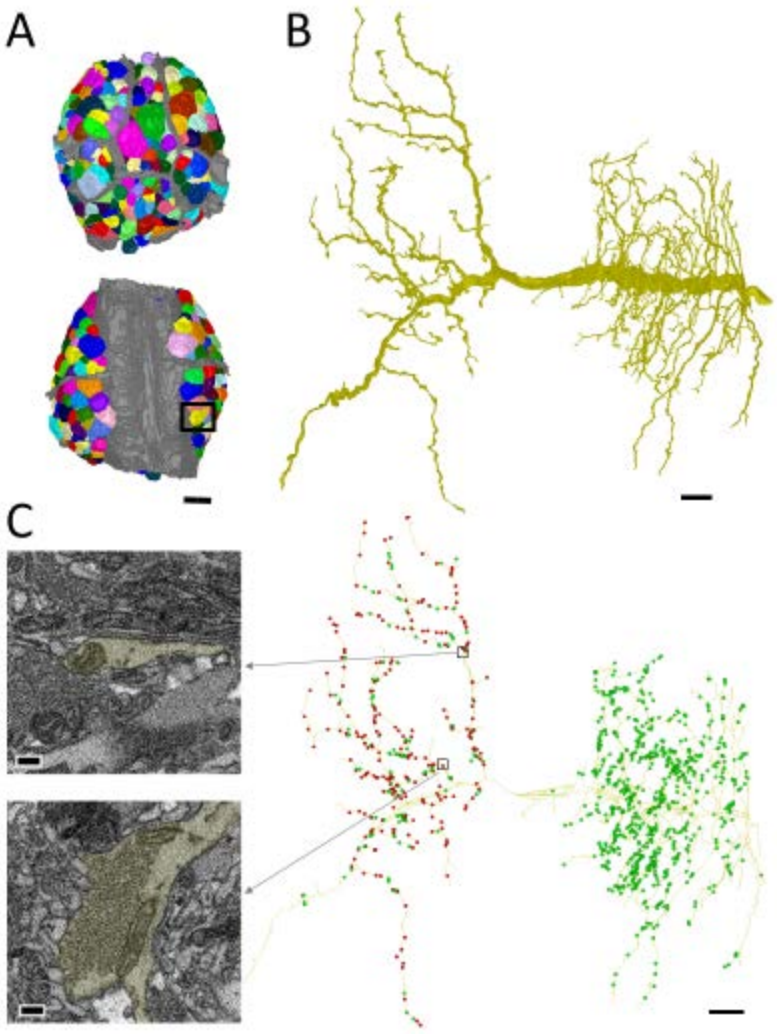

Figure 10. **The right DI-1.** A map of the entire ganglion can be used to identify, trace, and annotate full arbors. **(A)** A reconstruction of each neuronal soma in the ganglion (various colors) overlaid on the grey neuropilar and packet boundaries. **(B)** The fully reconstructed arbor of the right cell DI-1 (boxed in (A)). **(C)** Examples of a site of synaptic input and output and their location among all the synaptic inputs (green balls) and outputs (red balls) in the skeletonized arbor of the right cell DI-1. Scale bars 40µm in (A), 10µm in (B,C), 300nm in insets in (C).

Cell DI-1 is an inhibitory motor neuron that inhibits dorsal longitudinal muscles in the body wall directly as well as inhibiting excitatory motor neurons within the central neuropil (Ort et al., 1974; Cline et al., 1985). To determine whether the locations of synaptic input and output within cell DI-1 (Figure 10C) are a pattern common to other motor neurons, we

traced the inputs and outputs of other motor neurons, both inhibitors and excitors, of the same longitudinal muscles. Not surprisingly, we found that the DI-1 on the opposite (left) side, was a mirror image of the right DI-1 neuron, and that another inhibitor of the dorsal longitudinal muscles (the pair of DI-102 cells) also had a zone ipsilateral to the soma with extensive synaptic input and a contralateral zone of mixed inputs and outputs (Figure 11A). A pair of excitatory motor neurons to the same dorsal longitudinal muscles (DE-3 cells) lacked presynaptic vesicles throughout both their ipsilateral and contralateral arbors, with a few exceptions near the contralateral edge of the neuropil (Figure 11B). These connectivity patterns are consistent with physiological observations: cell DE-3 makes no known chemical synaptic connections (Ort et al., 1974), and cell DI-1 inhibits excitatory motor neurons exclusively by connections on the contralateral side (Lytton & Kristan, 1989). We also examined motor neurons which innervate the ventral longitudinal muscles. Cells VI-2 inhibit these muscles and excitatory motor neurons analogously to DI-1, and these cells also contain an ipsilateral portion of their arbor which is entirely postsynaptic and a contralateral portion of mixed postsynaptic and presynaptic function. Cells VE-4, a pair of excitatory motor neurons presynaptic to the ventral longitudinal muscles, are unique among leech neurons in having only an ipsilateral arborization (Fan et al., 2005). We found that their arbors contained only postsynaptic connections.

Not all inhibitory neurons segregated their input and output arbors on the left and right sides as did cells DI-1, DI-102, and VI-2. Cells 116, a pair of neurons that inhibit both dorsal and ventral motor neurons (EP Frady and K Todd, personal communication) arborize in both the ipsilateral and contralateral neuropil like these inhibitory motor neurons, but unlike them cells 116 had sites of synaptic input and output throughout both halves of its arbor

(Figure 11C). Similarly the S cell, an interneuron involved in the shortening reflex of the leech known to make only excitatory connections (Frank et al., 1975; Magni and Pellegrini 1978; Muller and Scott 1981), had both inputs and outputs throughout all the branches of its arbor (Figure 11D). These branches descend from the S cell's thick axon that travels outward in both directions from the ganglion in Faivre's nerve (Laverack 1969; Frank et al., 1975; Muller and Carbonetto, 1979).

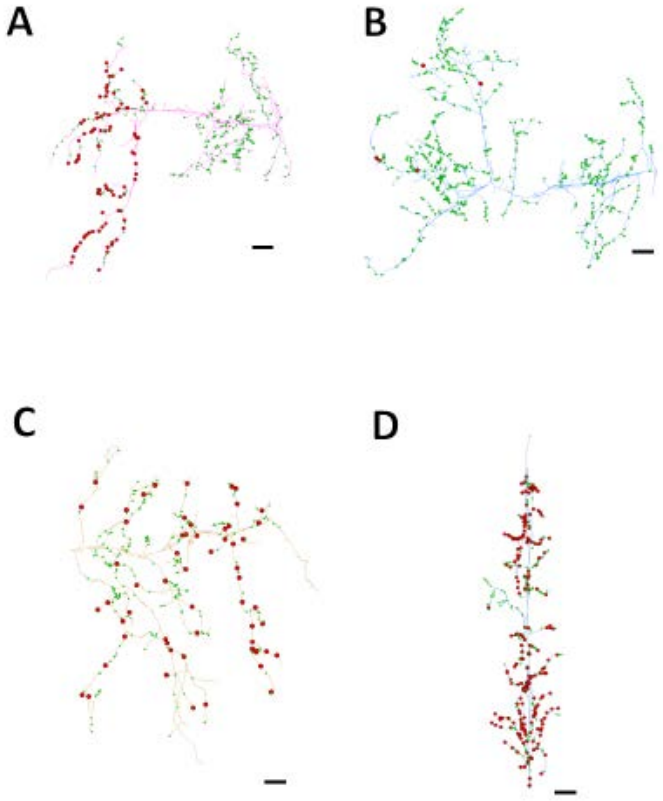

Figure 11. **Distributions of input and output sites**. In all panels green balls represent input sites and red balls represent output sites. **(A)** The skeleton arbor of the right DI-102 reveals outputs are lateralized to the contralateral half of its arbor while input sites are distributed throughout. **(B)** The skeleton of the right DE-3 is almost completely devoid of output sites within the ganglion with the exception of a few in the contralateral portion of its arbor. **(C)** The skeleton of the left cell 116 contains input and output sites intermingled throughout all branches of its arbor. **(D)** The S cell also has input and output sites on every branch of its arbor. Scale bars 10µm.

Discussion

Among the early investigators to use electron microscopy to investigate the leech nervous system, Coggeshall and Fawcett (1964) wrote of the neuropil: "The complexity of this region and the sampling problem inherent in electron microscopy make it impossible at present to provide a functionally meaningful account of the synaptic relationships within the neuropil, or even to identify the source of the various categories of nerve processes. Until means are devised for overcoming this sampling problem […] the morphologist must be content to describe the cytological characteristics of the glial cells and the fine structure of the various nerve processes and synaptic complexes encountered here." In our work, we applied SBEM in order to solve this "sampling problem" and begin describing the features of neuronal arbors within the ganglion's neuropil.

We sampled both a small section of adult neuropil and an entire juvenile ganglion (containing both the outer layer of cell bodies and the inner neuropilar zone). These are the first large serial EM datasets generated from leech. Within the juvenile volume, we were able to identify every soma of neurons in a midbody ganglion (ganglion 11). We report that the total number of cells in this ganglion is 397, in line with previous estimates of 350 (Ort et al., 1974) and 400 (Macagno 1980). Macagno (1980) counted neurons from several ganglia stained with osmium tetroxide and cut into thick serial sections. Using this approach he counted 400 neurons in ganglion 11, and a range of 389 to 398 neurons in ganglion 10. Our results corroborate the finding that small variability in cell number exists even in the same ganglion from animal to animal. We also corroborate Macagno's (1980) finding that despite the overall bilateral symmetry of the anterolateral and posterolateral packets, the right and left counterparts do not necessarily contain the same number of cells. This is not surprising

given that even large sensory neurons like the P cells that normally inhabit the posterolateral packets are sometimes encountered in the anterolateral, posterior, and central packets. Indeed, it seems likely that the precise location of a given soma is unimportant relative to the positioning and connections made by its arbor.

We also report the existence of seven neurons whose somata resided within the neuropilar compartment, just interior to the ventral bounding layer of the neuropilar capsule. This is not a new observation, as Coggeshall and Fawcett (1964) first noticed occasional neuronal somata in the neuropil as well. To our knowledge, however, the possibility that neurons can wholly reside in the neuropil has since been overlooked. It remains to be seen whether these cells are typically found in the neuropil or are somehow aberrant. We do not find any evidence of synapses onto the somata of these cells, so it may be the case that their overall structural organization is essentially similar to all other neurons. Within the adult neuropil volume, most arbors contained vesicles (87%), while the remainder (13%) lacked any. This fraction of vesicle-less arbors increased in the juvenile ganglion, where 22% of randomly sampled arbors lacked vesicles. It is unclear if this discrepancy is meaningful, or if it is due to a sampling artefact related to the adult sample's representation of approximately only 5% of the total adult neuropil. In the juvenile ganglion, we could trace entire arbors, revealing that some completely lack any vesicles or presynaptic varicosities (the VE-4s), or almost entirely lacked vesicles (the DE-3s). Other cells segregated their arbors, with the contralateral half full of vesicle-containing varicosities (DI-1s, VI-2s) while the ipsilateral half remained devoid of vesicles. Still others possessed vesicle-containing varicosities in every branch of their arbor (the inhibitory 116s, and the excitatory S cell). Leech neurons, like many invertebrate neurons, are monopolar and therefore lack obvious

dendritic and axonal compartments within the neuropil when compared to vertebrate neurons. However, the various combinations of vesicle-containing and vesicle-lacking processes in the arbors we traced suggests that the leech neurons nonetheless have the capability to spatially segregate their arbors into input-only zones and mixed input and output zones (notably, we found no example of an arbor or portion thereof that was only presynaptic to other cells).

Structurally, vesicle-lacking processes branched prolifically with many small extensions near the tips of branches that receive synaptic input from a contacting presynaptic varicosity belonging to another arbor. It was not uncommon to find processes of one of these arbors that contacted the same presynaptic bouton more than once, or that contacted multiple boutons belonging to the same presynaptic cell (see Figure 2E). Vesicle-containing arbors were diverse. Some contained primarily small presynaptic vesicles which were aggregated into fields within boutons and varicosities. These fields might be bounded by scattered larger vesicles (Figure 2A-C). This kind of arrangement is typical of what has been described before in the leech, where the larger vesicles have been described as neurosecretory granules (Coggeshall and Fawcett, 1964) or dense-cored vesicles (Muller and McMahan, 1976; Muller, 1979). These earlier efforts also distinguished the small presynaptic vesicles as being either granular or agranular (Muller and McMahan, 1976; Muller 1979) and work in the crustacean stomatogastric ganglion has similarly differentiated small vesicles on the basis of their size and shape (King 1976; Kilman and Marder, 1996). While such fine differences are likely present in our data, the resolution limits inherent to SBEM precludes us from making any classification scheme based on them. We do observe some differences in vesicle-containing arbors that become apparent when these can be

studied across many serial images. For instance, most of these arbors contain vesicles within boutons or varicosities that are linked by thinner processes (Figure 2E) and at these sites the presynaptic vesicles, larger vesicles, and mitochondria all densely fill the cytoplasm of the process (Figures 2, 3). Among the arbors we traced in the juvenile ganglion, cells 116, DI-1, VI-2, DE-3, DI-102 all display this pattern in their secondary branches. In some vesicle-containing arbors, vesicle fields did not fill their containing process, and often multiple smaller vesicle fields could be observed within the same section (Figure 4). In the juvenile ganglion, we observed this pattern in the S cell and the two interneurons known as the coupling interneurons because of how strongly electrically-coupled they are to the S cell (Muller and Scott, 1981).

While many arbors contained a population of scattered larger (100nm maximal diameter) vesicles surrounding their pools of small presynaptic vesicles, we found a few arbors that contained substantial aggregations of larger vesicles. With our staining protocol, there appear to be at least two basic types of these vesicles: intensely stained (maximal diameter 100nm) and lightly stained (maximal diameter 170nm). The intensely stained dark vesicles have been described previously as “vesicles with extremely dense, somewhat eccentric cores” and were speculated to contain monoamines (Muller, 1979). Coggeshall and Fawcett (1964) noted that certain somata that contained large aggregations of dense-core vesicles, a feature we also observed. Our results suggest that intensely-staining vesicles are found within the somata and processes of serotonergic neurons (Figure 9). While we cannot rule out additional neurotransmitters which might be present in these vesicles or produce a similar staining intensity, we note that the number and distribution pattern of somata containing them matches known serotonin staining (Kuffler et al., 1987; Lent et al.,

1991). Two of these cells are the Retzius cells, which have been previously shown to contain dense core serotonergic vesicles in their somata and at synaptic sites (Kuffler et al., 1987; Trueta et al., 2012).

The population of large lightly-stained vesicles has not been previously differentiated from other presumed neurosecretory vesicles (though there are images of them [Plate 33 in Coggeshall and Fawcett, 1964]). We found these vesicles concentrated in the somata of eight neurons, including what we identify as the Leydig cells on the basis of soma size and position.

Both the intensely-stained and light-staining large vesicles were found in four arrangements: in aggregations surrounding fields of smaller vesicles, in aggregations by themselves within the arbor, in aggregations by themselves in the soma, or in isolation within the arbor. It is unclear which of these arrangements, if any, are most likely to be sites of exocytosis. Aggregations within the arbor, particularly those which surround small vesicle fields, seem to be likely candidate sites. The aggregations of these vesicles in the somata probably indicate that the soma plays a major role in producing and storing them. However, previous work has shown that, in the Retzius cells, large dense-core vesicles can be released from the somata themselves (Trueta et al., 2012). Isolated vesicles are also widespread: while we have not fully traced the Retzius cells in our volume, visual inspection of some its processes suggests that its intensely-stained vesicles are present in isolation throughout the main branches and within many of the smaller secondary branches. The presence of isolated vesicles in the main branch could be indicative of trafficking from the soma to eventual release sites in peripheral terminals outside the ganglion. The existence of isolated vesicles in the smaller branches is more intriguing, especially in those branches that do not otherwise

lead to a presynaptic bouton or any aggregation of vesicles at all. It is possible that these vesicles can be released anywhere, or that these neurons have relatively lax trafficking rules which result in these vesicles entering processes within which they have no functional role. Notably, when Kuffler et al. (1987) tested uptake in the cultured Retzius cells, they found that extracellular horseradish peroxidase was taken up throughout the cell, rendering it dark even at the light level. These observations underscore a major challenge in connectomics: it is difficult to determine where exactly the contents of neurosecretory vesicles are released or which of the myriad arbors nearby are influenced by the diffusion of their contents.

At traditional synapses, it was possible to identify the presynaptic and postsynaptic arbors. We classified chemical synapses on the basis of existing conventions (Muller and McMahan, 1976; Muller 1979) and subsequently studied the 3-dimensional features of the presynaptic varicosities and postsynaptic arbors apposed to them (Figure 2). We note that there is considerable variability within and between arbors with respect to the size of vesicle fields in a given varicosity. Generally, larger vesicle fields belonged to presynaptic varicosities with more postsynaptic targets (Figure 8). The typical leech synapse involves a larger presynaptic structure apposed to many postsynaptic processes (median of 7 in a random sample of presynaptic boutons within the adult neuropil, Figure 8). This contrasts with the typical arrangement of the vertebrate neuropil, where a single bouton contacting multiple postsynaptic partners is unusual (Wilke et al., 2013; Kasthuri et al., 2015).

The ability to trace full arbors and locate the synaptic connections among them is one of the great promises of SBEM and ssTEM and is essential for connectomics (e.g. White et al., 1986; Bock et al., 2011; Briggman et al., 2011; Helmstaedter et al., 2013; Randel et al., 2014; Ohyama et al., 2015). In the subsequent chapter, we discuss our efforts to confirm,

challenge, and discover synapses among arbors fully reconstructed from the juvenile ganglion volume. However, the dividends of SBEM and ssTEM extend beyond analysis of connectivity. The potential to reconstruct the full structure of neurons and their intracellular components also offers rich rewards. Reconstructions from serial EM datasets can be used to predict the diffusion of molecules in the extracellular spaces of neuropil (Kinney et al., 2013), the diversity of presynaptic structures (Wilke et al., 2013), or locate proteins of interest tagged with markers that differentiate them in EM (Deerinck et al., 2013; Atasoy et al., 2014; Lam et al., 2015). Here we focused on describing the diversity of vesicle arrangements and localization of presynaptic boutons and synaptic inputs found within arbors of leech neurons. This information can in turn be used to identify neurotransmitter contents (in the case of the serotonergic intensely staining dark vesicles) or reveal which portions of an arbor receive only synaptic inputs and which also generate outputs. These factors are essential to understanding the functioning of a given neuron. The location of synaptic inputs relative to the production of synaptic outputs determines in part how strongly presynaptic neurons influence their postsynaptic partners. Retaining this 3D neuronal information therefore can only strengthen what would otherwise be reduced to one dimension in a connectome, and is essential to understanding how neural circuits produce behavior.

Chapter 2 represents work being prepared for publication. Jason Pipkin, Eric Bushong, Mark Ellisman, William Kristan. The dissertation author was the primary investigator and author of this material.

Chapter 3. Verifying, challenging, and discovering new synapses among fully EM-reconstructed neurons in the leech ganglion.

Abstract

In order to understand how neural circuits produce behavior, it is necessary to learn the precise pattern of synaptic connectivity among the neurons involved. For large numbers of neurons, it becomes difficult to establish such "connectomes" by physiological means, yet physiological accessibility is ultimately required to verify and measure synapses. We collected a volume of images spanning an entire ganglion of the juvenile leech nervous system via serial blockface electron microscopy (SBEM). We use this volume to identify and reconstruct known cells and to anatomically identify the synapses among them. We show that we can find numerous synaptic contacts between neurons previously known to be synaptic partners. We also find one case where a connection thought to exist by means of physiological recordings was not recovered anatomically. We also demonstrate that a synapse found within the EM volume can be recapitulated physiologically. Together these findings demonstrate the potential for connectomics in the leech nervous system: the harmony of anatomical detail and physiological precision provides unprecedented power for gaining understanding of how neural circuits in the leech are wired together.

Introduction

The behavioral repertoire of a given neural circuit is constrained in part by the connectivity pattern of the neurons in that circuit. In order to understand how circuits produce behavior it is therefore necessary to know which neurons make synapses onto which other neurons. In the medicinal leech, *Hirudo verbana*, many behaviors are produced by a chain of homologous ganglia containing approximately 400 neurons. To date, most of the work uncovering the circuitry responsible for given behaviors in the leech has relied on intracellular electrophysiology (e.g. Nicholls and Baylor, 1968; Ort et al., 1974) or optical monitoring of voltage-sensitive dyes (e.g. Briggman et al., 2005). These experiments have resulted in several well-characterized synapses and circuits (e.g. Ort et al., 1974; Stent et al., 1979; Lockery et al. 1990). Yet many neurons in the leech ganglion remain completely uncharacterized. Thoroughly characterizing the synaptic connectivity of every neuron in the ganglion by means of intracellular electrophysiology is infeasible due to the number of neurons involved.

Anatomical characterization of synaptic connectivity heretofore has largely been the province of light microscopy. For instance, in many systems it is possible to fill or label with fluorescent proteins a cell of interest and localize its synaptic contacts by further fluorescent labeling of synaptic proteins (e.g. Dani et al., 2010). In mammalian systems, light microscopy has been used to determine the synaptic connectivity of individual cells by the use of genetically engineered rabies and herpes viruses (Wickersham et al., 2007; Lo and Anderson, 2011). In the leech, a relatively paucity of genetic tools precludes these approaches. Therefore studying synaptic connectivity in the leech using light microscopy relies on comparing the overlap of at least two dye-filled neurons. In some cases, this light-level

approach is sufficient to disprove a direct connection when arbors do not overlap (Muller and Scott, 1981). In most cases, however, the arbor overlap between pre- and postsynaptic cell is extensive. While it is possible to estimate an upper bound on the number of synapses formed in a given pair in this way (see DeRiemer and Macagno, 1981), it is impossible to determine with light level cell fills which regions of overlap are truly synapses and which are the result of two processes coming very close but not touching (or touching but not forming a synapse). Determining the location and number of synaptic contacts precisely thus requires an approach with higher resolution.

Serial section electron microscopy provides the image resolution necessary to fully reconstruct neural circuits. For instance, the entire *C. elegans* hermaphrodite nervous system was reconstructed in the late 1970s and 1980s (White et al., 1986). Yet the time-consuming nature of this approach has, until recently, dissuaded attempts to apply serial EM to larger volumes of tissue. However, in the past decade the development of serial blockface scanning electron microscopy (SBEM) and various forms of serial section transmission electron microscopy (ssTEM) has dramatically reduced the image acquisition time spanning large volumes of neural tissue. The resulting datasets have been used to provide insight into both existing and novel circuits. Among others, these results include discovering new features of a known retinal circuit (Briggman et al., 2011), the complete circuitry of the tail of male *C. elegans* (Jarell et al., 2012), a new type of retinal bipolar cell (Helmstaedter et al., 2013), the complete visual circuitry of a flatworm (Randel et al., 2014), and the discovery of circuits responsible for turning behavior in larval *Drosophila* (Ohyama et al., 2015).

We applied SBEM to leech tissue in order to study known circuits and discover new synaptic connections. We previously reported on the distribution and pattern of synaptic

sites in two SBEM datasets: one small volume of mature leech neuropil, and one entire ganglion taken from the smaller yet behaviorally-mature juvenile leech (Chapter 2). Herein, we report on the connectivity uncovered within the juvenile ganglion dataset. In order to validate the approach, we first analyze the connections of well-characterized motor neurons that innervate the longitudinal muscles and participate in the swimming behavior. Secondly, we use the dataset to identify a previously uncharacterized synaptic relationship and subsequently verify it physiologically. Our results demonstrate the utility and potential of EM-based circuit reconstruction in the medicinal leech.

Materials and Methods

Animals

We used both adult and juvenile medicinal leeches, *Hirudo verbana.* Adult leeches were obtained from Niagara Leeches (Niagara Falls, NY) and housed in aquaria on 12 h daily light/dark cycle at 15-16°C. Juvenile leeches were obtained by harvesting cocoons produced by a breeding colony of adult leeches maintained in our laboratory. Leeches were allowed to mature within the cocoons at RT and collected once they had emerged. We then waited two weeks to ensure full development prior to dissection. We confirmed that the juveniles lacked any embryonic features using established staging criteria (Reynolds et al., 1998).

Sample preparation

Both adult and juvenile samples were prepared with the same protocol. We anesthetized the leeches in ice-cold leech saline (4°C) containing 115mM NaCl, 4 mM KCl, 1.8mM $CaCl_2$, 2mM $MgCl_2$, 10mM HEPES buffer (Nicholls and Purves, 1970). Midbody ganglia were then dissected from the nerve cord and pinned them to the bottom of Sylgard-coated

dish. The ganglia were then fixed for two hours RT in 2% PFA, 2.5% glutaraldehyde, and .1M phosphate buffer. After that the ganglia were rinsed in .1M phosphate buffer and incubated in 2% OsO_4 / 1.5% potassium ferrocyanide. For this step, the samples were microwaved in a scientific microwave three times with a duty cycle of 40s on and 40s off at a measured temperature of 35°C and subsequently left to sit at RT for thirty minutes. Samples were then washed in ddH_2O and microwaved three times with a 2 minutes on and 2 minutes off duty cycle at 30°C. We found that this and subsequent brief microwave incubations facilitated staining penetration to the center of our samples and was necessary to gain sufficient image contrast. Samples were then incubated in 1% thiocarbohydrazide (EMS) and microwaved three times with a 40s on and 40s off duty cycle at 30°C and subsequently left to incubate for 15 minutes RT. The samples were then washed again with the same microwave incubation as described earlier. Next, the samples were incubated in 2% aqueous OsO_4 and microwaved three times with a 40s on and 40s off duty cycle at 30°C and then incubated at RT for one hour. After washing, the samples were then left in 1% uranyl acetate overnight at 4°C. The next day, samples were incubated in a lead aspartate solution prepared by dissolving 0.066gm of lead nitrate into 10ml of 0.003M aspartic acid with the pH subsequently adjusted to 5.5 using 1N KOH. This incubation took place in a 60°C oven for 30 minutes. Next, the samples were washed and dehydrated through a series of ethanol solutions (50%, 70%, 90%, 100%, 100%, 10 minutes each) at RT and finally in acetone. Next, samples were infiltrated with plastic by first incubating them for two hours at RT in a solution of 50% acetone and 50% Durcupan and then overnight in 100% Durcupan. The next day, samples were transferred to a freshly prepared 100% Durcupan solution and incubated at RT for 2 hours. Samples were then incubated within a 60°C oven for three days. Durcupan Araldite resin was

made by mixing 11.4g of component A, 10g of component B, 0.3g of component C, and 0.1g of component D.

Imaging

The plastic-embedded ganglia were preserved within carefully-trimmed plastic blocks. For the juvenile sample, the edges of the block were trimmed until very near to the external capsule of the ganglion in order to reduce charging in the outer image tiles that would contain both tissue and empty plastic. Blocks were mounted onto pins to which they were adhered with conductive silver paint. The pin and block were then sputter coated with a thin layer of gold and palladium to further enhance conductivity.

The entire juvenile ganglion was imaged on a Zeiss MERLIN SEM equipped with a GATAN 3VIEW SBEM system. We collected montages of 8000x8000 raster tiles at 5.7nm pizel size. We oriented the sample so that it was imaged from the dorsal surface to the ventral surface with sectioning occurring perpendicular to the dorsal-ventral axis. Montage size thus varied from 1x1 to 5x5 tiles depending on how large the area of tissue was that was exposed to the surface of the block. We sectioned the block 2203 times at 50, 100, or 150 nm thicknesses. The 100nm and 150nm sections were taken in regions containing only cell bodies (at the top and bottom of the overall volume) as there were no fine neuronal processes to trace here and thus imaging time could be reduced. Similarly, we varied dwell time throughout acquisition along a range of 0.8µs to 1.5µs with higher dwell times used in neuropil-containing sections. During the juvenile ganglion acquisition, an unexpected and gradual reduction of contrast gradually occurred due to an unexpectedly early degradation of the filament in the electron gun. We therefore focused most of our analysis and reconstruction on cells whose arbors tended to fall within the dorsal half of the ganglion.

Reconstruction

In the juvenile ganglion volume, montages and sections were aligned using TrakEM2 (Cardona et al., 2012). Subsequent tracing and annotation was also performed in TrakEM2. In this volume we largely traced arbors via skeletonization rather than full segmentation of everything within a given neurons plasma membrane.

All tracing, segmentation, and analysis was performed by JP. In order to reduce errors, the arbors of the motor neurons discussed in Figures XXXX were reviewed at least twice. As has been previously reported we found that false negatives (missing branches) were far more likely errors than false positives (adding the wrong branch) (Ohyama et al., 2015).

Electrophysiology

Adult leeches were anesthetized in ice-cold saline, dissected, and chains of four midbody ganglia were removed and pinned in Sylgard-coated dish. The ventral sheath of the second ganglion and dorsal sheath of the third ganglion were removed to expose cell bodies for penetration with 1.0mm X 0.75mm glass microelectrodes with an omega dot pulled to a resistance of ~20MΩ. Microelectrodes were filled with 20mM KCl and 1 M potassium acetate. To verify that the S cell was impaled, the connective between the third and fourth ganglia was recorded with an extracellular electrode. To verify cell 116's identity, we loaded electrodes with either Alexa Fluor 488 or Alexa Fluor 594 (Thermo Fisher Scientific) and backfilled with 3M potassium acetate. Dye was then injected with alternating depolarizing and hyperpolarizing current pulses (2nA for 300 ms, -2nA for 50ms, 10% duty cycle for 30 minutes) and the shape of the arbor compared to the reconstructed arbor from the juvenile ganglion SBEM dataset.

Intracellular current injection and measurement of membrane potential were mediated by an Axoclamp-2B amplifier (Axon Instruments, Inc.) operated in bridge mode. Extracellular recordings were amplified by a Model 1700 A-M Systems differential amplifier. Electrical signals were digitized and recorded and analyzed with WinWCP (Strathclyde Electrophysiology Software). Further analysis was performed with Microsoft Excel (Microsoft).

Results

Testing physiologically-characterized circuits anatomically

The synaptic connections among neurons that generate behaviors in the leech are made within the neuropil of each ganglion. Within our juvenile ganglion volume, we explored the connections of a subset of motor neurons known to participate in the swimming behavior (Ort et al., 1974). Specifically, we searched the neuropil for synapses among pairs of neurons DI-1, VI-2, DI-102, DE-3, and VE-4, which innervate dorsal and ventral longitudinal muscles and are responsible in part for the undulation of the leech's body during swimming. In addition, we also searched for connections made by these cells with the pair of L motor neurons, which are excited during the shortening reflex but are inhibited throughout swimming.

The physiologically-determined circuit among these cells is depicted in Figure 1A. (adapted from Ort et al., 1974). In this diagram, non-rectifying electrical synapses are represented by resistors and rectifying electrical synapses are represented by diodes. As the resolution of SBEM precludes the direct observation of gap junctions, we turned our attention first to chemical synapses. In Figure 1A, chemical synapses are represented by

lines with either a ball at the end (signifying an inhibitory connection) or a T-junction (signifying an excitatory connection). We first sought to locate and quantify the number of known inhibitory synapses made within the neuropil in this circuit. To do so, we manually traced skeleton arbors of all the neurons involved, noting where each neuron made a synapse onto the other neurons, using the criteria established in our previous study (Figure 1B,C) (Chapter 2). The number of synapses formed in this network are summarized in the connectivity matrix shown in Table 1. We found numerous synaptic contacts consistent with the previously-described direct inhibition of DE-3 by the ipsilateral DI-1 and D1-102 and the direct inhibition of VE-4 by the ipsilateral VI-2. We did not find any chemical synapses from DI-1, DI-2, or DI-102 onto either L cell (Figure 1B), suggesting that the observed physiological inhibition occurs via an indirect pathway (potentially via the electrical connections).

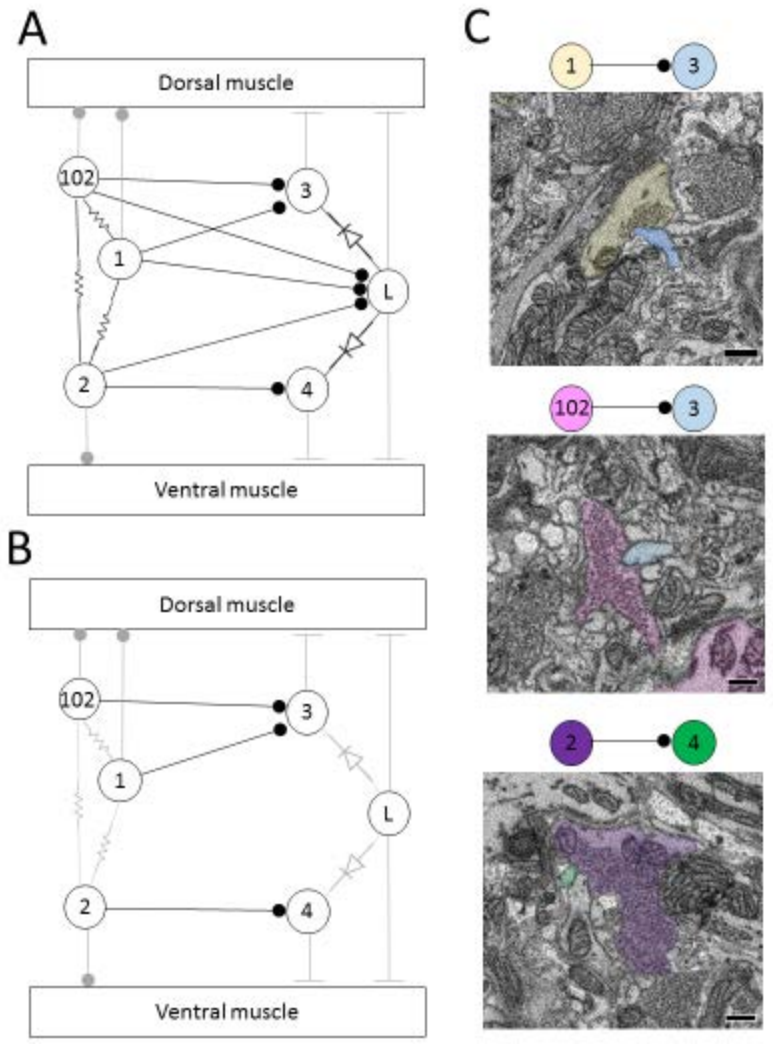

Figure 1. **Confirming a known circuit.** Many, but not all, of the predicted physiological connections were recovered anatomically after reconstructing the arbors of seven pairs of dorsal motor neurons. **(A)** Predicted circuitry based on electrophysiology, adapted from Ort et al. (1974). Lines ending in circles represent inhibitory connections; lines ending in a flat line indicate excitatory connections; resistors indicate non-rectifying gap junctions; diodes represent rectifying gap junctions. **(B)** Updated circuitry based on what was directly observed after anatomical reconstruction. Electrical connections are grayed out as these are not directly observable with SBEM. All predicted connections were found except those onto the L cell. **(C)** Examples of synapses between the right DI-1 and the right DE-3, the right DI-102 and the right DE-3, and the left VI-2 and the right VE-4. Scale bars 300nm.

Table 1. Connectome. Number of chemical synaptic contacts found among six pairs of motor neurons. Presynaptic cells are listed in the first column and postsynaptic cells are listed in the first row. All expected connections were found, with the exception of direct connections from DI-1, DI-102, or VI-2 onto the L cells. Some unexpected synapses were also found but were typically low in number compared to expected synapses (e.g. right DI-1 onto left DE-3).

	Right DI- 1	Left DI-1	Right VI-2	Left VI-2	Right DE-3	Left DE-3	Right VE-4	Left VE-4	Right DI-102	Left DI-102	Right L	Left L
Right DI- 1			2	2	18	1		1				
Left DI-1						9				3		
Right VI-2					2			2				
Left VI-2							5					
Right DE-3												
Left DE-3												
Right VE-4												
Left VE-4												
Right DI-102					17			1				
Left DI-102		2				16						
Right L												
Left L												

As suspected from physiological recordings (Ort et al., 1974, others), we observed that each DE-3 received direct inhibitory input from the ipsilateral DI-1. We previously observed that each DI-1 only forms presynaptic boutons in the contralateral portion of their arbors (Chapter 2). In Figure 2A, the right DI-1 (green) is presynaptic to the right DE-3 via 18 synapses (teal dots). Within the contralateral arborization of DE-3, these 18 synapses were

widely distributed (Figure 2B), contradicting previous predictions that inputs from DI-1 might be concentrated onto a single branch (Lytton & Kristan, 1989). We found a similar pattern among the inputs from the DI-102s onto the DE-3s (data not shown). Notably, the right DE-3 received no input from the left DI-1, despite overlap of the vesicle-containing portion of the left DI-1's arbor with the ipsilateral arborization of the right DE-3 (dashed ellipse, Figure 2C). With one exception, this was also true for the right DI-1 and left DE-3 and for both DI-102s and DE-3s (Table 1). Similar to the dorsal muscle inhibitory motor neurons (DI-1 and DI-102), the ventral inhibitor (VI-2) neurons form presynaptic boutons in only the contralateral portion of their arbor. Consistent with the fact that the pair of ventral excitatory motor neurons (VE-4) arborize exclusively in the in the ipsilateral half of the neuropil each VE-4 received direct inhibition only from the contralateral VI-2 (Table 1), a finding that confirms electrophysiological characterization of this connection (Ort et al., 1974).

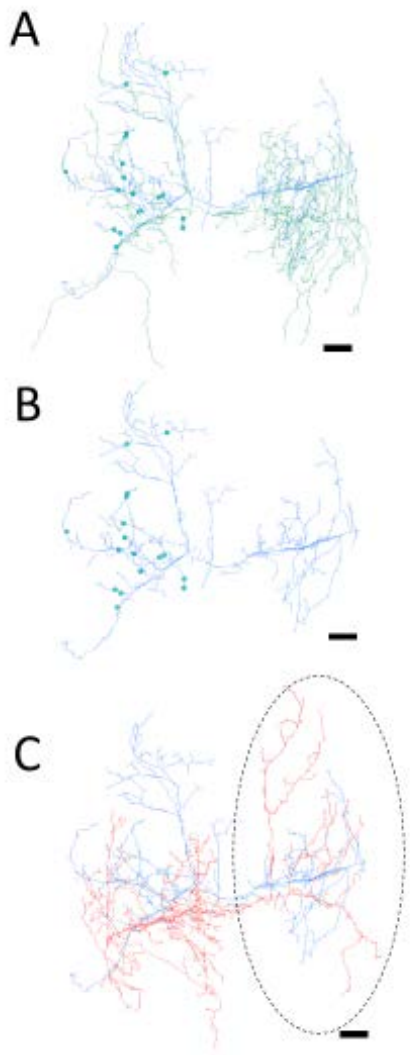

Figure 2. Overlap not predictor of connectivity. The right DE-3 receives numerous widely-distributed synaptic inputs from the right DI-1 and none from the left DI-1. **(A,B)** The right DE-3 (blue skeleton) receives synaptic input from the right DI-1 (green skeleton) at 18 sites (green dots) widely distributed throughout the contralateral half of its arbor. **(C)** The left DI-1 arbor (red skeleton) overlaps with the right DE-3 arbor. Even where the left DI-1 forms presynaptic boutons and the right DE-3 receives synaptic inputs, no synapses are found (region within dashed oval). 10µm scale bars.

Electrical connections

It is impossible to directly observe the fine structures characteristic of gap junction membrane appositions (Brightman and Reese, 1969) when constrained by the resolution

limits of SBEM. Nonetheless, we knew that several of the cells we traced formed electrical connections with each other on the basis of prior physiological evidence. We therefore took note when the membranes of two cells known to be electrically-coupled came into extended contact over many sections. On the basis of this criterion, we observed several suggestive contacts. In some cases, the contact is extensive in area and seen at many separate sites. For example, we traced the S cell, a unique excitatory interneuron involved in the shortening reflex (Levarack 1969; Frank et al., 1975; Magni and Pellegrini, 1978) and known for its large fast-conducting axon that it extends both anteriorly and posteriorly in Faivre's nerve. Halfway between each ganglion, this axon forms an electrical synapse with the S cell of the adjacent ganglion such that spikes generated in one S cell are propagated throughout the entire nerve cord (Muller and Carbonetto 1979). Additionally, the S cell is known for making strong electrical connections with two "coupling interneurons" that act in part as relays for sensory inputs (Muller and Scott, 1981). In Figure 3A, we show a confluence of processes belonging to the S cell (blue) and one of each coupling interneuron (green and pink). In this particular junction, each cell's membrane is closely apposed to and conforms to each other's and this interaction persists over several sections. We also searched for contacts among other known coupled cells. For example, Figure 3B depicts the close apposition of the left DI-102 (red) and left DI-1 (yellow). Both these cells are known to be physiologically coupled (Figure 1A). Here two of their secondary branches come into close contact as they travel adjacent to each other; notice again that both cells' membranes are closely apposed and conformed to each other. Not all possible junction sites involved symmetrically sized processes. In one case, a thin process belonging to the left DE-3 (teal) burrows into the primary process of the right DE-3 (blue) (Figure 3C). Again, both these cells are known to be

coupled (almost all pairs of dorsal motor neurons are electrically coupled [Ort et al., 1974; Fan et al., 2005]). In every instance involving known electrically coupled cells, we observed sites of membrane contact that could harbor gap junctions. For instance, we found 24 and 26 contacts between the S cell and each coupling interneuron, 5 between the left DI-1 and left DI-102, and 10 between both DE-3s. Like chemical synapses (Figure 2A,B), these contact sites were distributed throughout cell's arbors.

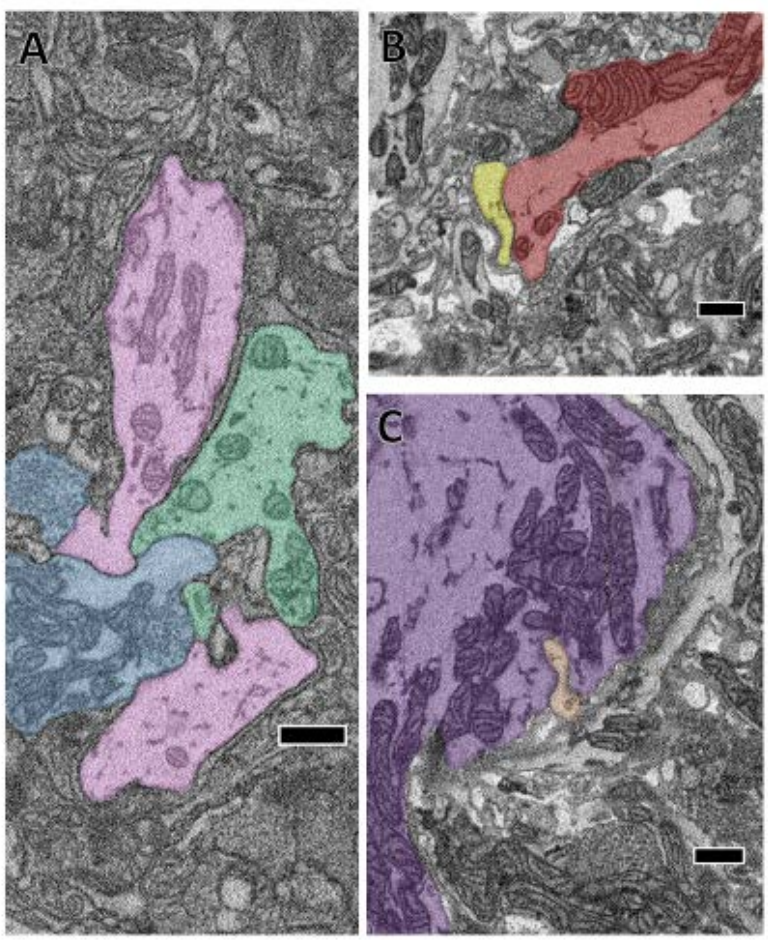

Figure 3. **Gap junctions.** The close apposition of cell pairs known to be electrically coupled could harbor gap junctions. **(A)** The confluence of the S cell (blue) and both coupling interneurons (pink and green). **(B)** Close apposition between two processes of the left DI-102 (red) and left DI-1 (yellow). **(C)** A small branch of the left DE-3 invaginates the main branch of the right DE-3. Scale bars 500nm in all.

Predicting a physiological connection from an anatomical connection

By analyzing this physiologically well-characterized motor-neuronal circuit, we were able to confirm the anatomical existence of many of the connections predicted from previous electrophysiological studies, and disconfirm others. We next sought to perform the inverse experiment: does an anatomical synapse predict a physiological connection? For this experiment, we turned to cell 116. Each cell 116 is inhibitory and resides in the dorsal aspect of the anterolateral packet (Frady and Todd, personal communication). In tracing arbors of the pair of cells 116, we noticed that each received synaptic input from the S cell. The S cell (blue skeleton, Figure 4A) made 6 synapses onto the right 116 (orange skeleton, Figure 4A) and 7 synapses onto the left 116 (green skeleton, Figure 4A), distributed throughout the extent of the S cell arbor (pink dots, Figure 4A). In one case, both cells 116 were postsynaptic to the same S cell bouton.

We next tested to see if inducing action potentials in the S cell network would reliably produce monosynaptic excitatory postsynaptic potentials in cell 116. Because the S cell in one ganglion is strongly coupled to the S cells in the next ganglion anterior or posterior to it, we were able to circumvent the practical difficulty of simultaneously recording intracellularly from one cell on the ventral surface and another cell on the dorsal surface. Instead, we impaled the S cell in the ganglion adjacent to the one in which we recorded cell 116 (Figure 4C). To confirm that the spike traversed through the network, we recorded the connective nerves posterior to the cell 116 ganglion with an extracellular electrode (Figure 4C). We observed that each S cell spike reliably produced a 1-2 mV EPSP in cell 116. The cell 116 response to 15 spikes (overlaid, grey traces in middle panel) is presented in Figure 4C along with their average (black trace in middle panel). The 4-5ms latency between spike and

EPSP is consistent with known conduction velocity of the S cell spike through Faivre's nerve (Frank et al., 1975).

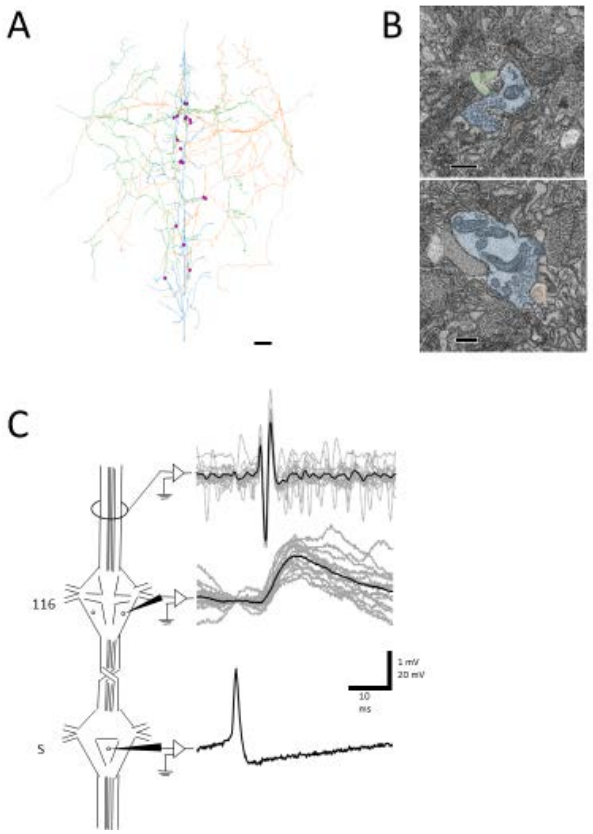

Figure 4. **Discovering a new synapse.** A synapse discovered anatomically can be verified physiologically. **(A)** Skeleton arbors of the presynaptic S cell (blue) and postsynaptic cells 116 (green and orange) with pink dots representing sites of synaptic contact. 10µm scale bar. **(B)** Examples of synapses from S onto the left 116 (top) and right 116 (bottom). 300nm scale bars. **(C)** Recordings in adult nervous system. Spikes were induced in the S cell in one ganglion (bottom trace) whereupon they traveled across the S cell network down the nerve cord, eliciting a reliable depolarization in cell 116 (middle trace). The S cell spike was visible in an extracellular recording of the connective nerves posterior to the ganglion containing the recorded 116, indicating that the spike successfully passed through (top trace). A single spike in the S cell is presented for clarity in the bottom trace while the middle and top represent recordings following 15 separate spikes from the same preparation (grey) and their average (black).

Discussion

Our results validate a connectomics approach for circuit discovery in the leech ganglion. We show that reconstruction of selected cells can be used to confirm the existence of previously known connections among motor neurons (Figure 1, Table 1). Previous work showed that the ipsilateral DI-1 and DI-102 monosynaptically inhibit DE-3, while the contralateral VI-2 inhibits VE-4 (Ort et al., 1974; Granzow et al., 1985). At the resolution of light microscopy, previous reports have observed considerable overlap between the processes of these cells and have noted possible sites of apposition of postsynaptic processes with presynaptic varicosities (Granzow et al. 1985, Fan et al., 2005). At the EM level, Granzow et al. (1985) attempted to demonstrate the connection between DI-1 and DE-3 by differentially staining the two cells (Imposil in DI-1, horseradish peroxidase in DE-3) and taking thin sections of the contralateral half of the neuropil. However, due to suspected disruption of vesicle structure wrought by Imposil they found presynaptic vesicles near only one of many sites of abutment between the two cells (Granzow et al., 1985). By collecting a complete SBEM volume of an entire ganglion, our report is the first to provide direct EM anatomical confirmation of these synapses among motor neurons.

For each of these known connections (DI-1->DE-3, DI-102->DE-3, VI-2->VE-4) we found more than one synapse from the presynaptic cell onto the postsynaptic cell. The number of such contacts ranged from 2 (from the right VI-2 onto the left VE-4) to 18 (from the right DI-1 onto the right DE-3) (Table 1). It's unclear in what ways this variability is physiologically meaningful as we cannot infer the synaptic strength of a given synapse in a SBEM volume. The range of contact number we observe falls below that measured by light microscopic analysis of overlap between adult sensory and motor neurons (13-41 in

DeReimer and Macagno, 1981). This difference could be due to the maturity of the tissue, the specific cell pairs studied, or methodological differences (processes may overlap at the light level that do not touch at the EM level).

We did observe some unexpected sites of potential synaptic contact among the motor neurons we traced (for example, the right DI-1 makes a single synapse onto the left VE-4). Notably, these cases involve far fewer overall contacts. There are a number of possible explanations for these aberrations: (1) these synapses could be real but so relatively few in number as to be physiologically undetectable and unimportant, (2) these synapse might only be present in juvenile tissue that could still be undergoing synaptic refinement, (3) these synapses could be mistakenly identified or otherwise be the result of a tracing error that we cannot detect after reviewing them.

We found that synapses between two cells widely spanned the region of overlap between the vesicle-containing portion of the presynaptic cell's arbor and the postsynaptic cell's arbor (Figure 2). Earlier reports had suggested that the synapses made by DI-1 and DI-102 might be concentrated onto separate single branches of the DE-3 arbor (Lytton and Kristan, 1989). We find no evidence for such selectivity in our juvenile ganglion volume, though we cannot rule out that synapse strength might vary depending on where a synapse occurs or that branch-selectivity is a process that is not yet complete in juvenile tissue. Most neurons in the leech ganglion are paired, having both a left and right homolog (Ort et al., 1974). In the case of the motor neurons studied here, these bilateral homologs are all strongly electrically coupled (with the exception of the VE-4 cells, whose arbors do not span the midline and therefore are uncoupled) (Fan et al., 2005; Ort et al. 1974). Given this pattern of connectivity, it is interesting to note that we almost exclusively found synapses

from the DI-1 and DI-102 cells onto the ipsilateral DE-3 even though the vesicle-containing portion of the DI-1 or DI-102 arbor overlaps with postsynaptic regions of both the ipsilateral and contralateral DE-3. We found only one synapse that broke this lateral selectivity pattern, from the right DI-1 to the left DE-3 which stands in contrast to the 18 synapses found from the right DI-1 to the right DE-3 (Table 1). This lateral selectivity suggests that there may be some chemical basis by which synapse formation is restricted to the ipsilateral cell pair. For example, it could be possible that the DE-3s preferentially express the molecules required for synapse formation with DI-1 and DI-102 in the contralateral half of their arbor. This result also underscores the strengths of EM versus light microscopy: arbor overlap is not predictive of where synapses occur. As more serial EM datasets are published, this appears to be true in other systems as well. In the retina, random synapse formation on the basis of process proximity cannot explain the location of synapses found between direction-selective cells and starburst amacrine cells (Briggman et al., 2011). Similarly, recently Kasthuri et al. (2015) report that proximity of axons to dendritic spines was a poor predictor of connectivity in an ssTEM dataset spanning a volume of the mouse neocortex.

The presence and pattern of synapses we found among DI-1, DI-102, VI-2, DE-3, and DE-4 conformed to our expectations given known physiological evidence (Ort et al., 1974). However we failed to find any synapses from DI-1, DI-102, or VI-2 onto either L cell as previous physiology predicted (Table 1) (Ort et al. 1974). The L cell is known to be electrically coupled to other excitatory motor neurons which receive direct monosynaptic inhibition from DI-1, DI-102, and VI-2 (Ort et al., 1974, Fan et al., 2005). Therefore, the synaptic input from these cells onto the L cell may be indirect while physiologically appearing otherwise. This finding underscores the utility of anatomical synapse verification at the EM level:

physiologically monosynaptic connections between cells whose arbors overlap are nonetheless not necessarily directly monosynaptic.

Detecting electrical connections mediated by gap junctions remains an unsolved challenge in SBEM-based connectomics. In our volume, we knew certain cell pairs to be coupled, and were able to locate several places where their membranes came into prolonged contact (Figure 3). Some of these sites are almost certain to contain gap junctions, but we cannot determine how many are functional versus incidental. In the future, techniques to preserve or expand the extracellular space between neural processes may eliminate most of the incidental contacts while preserving locations where cells are truly coupled. This, in concert with post hoc physiological verification, could lead to the description of patterns of membrane apposition associated with gap junction presence even in relatively lower resolution images.

Connectomics generates anatomical predictions of neural connectivity which can then be verified physiologically. In the larval fly, Ohyama et al. (2015) recently used connectomics to predict a neuronal circuit responsible for multisensory integration involved in rolling behavior. They then verified predicted connections using calcium imaging. Similarly, we demonstrated that anatomical connections can be recapitulated in physiological measurements by first discovering synapses from the S cell onto both cells 116 in our EM volume and then subsequently demonstrating that spikes in the S cell produce a monosynaptic excitatory postsynaptic potential in cell 116 (Figure 4). This result also highlights the advantages of using an electrophysiologically accessible system in which the same cells can be identified from ganglion to ganglion and animal to animal. In principle, a

complete reconstruction of every cell in a ganglion could similarly be physiologically tested by pairwise recordings in other ganglia.

While the leech is studied in part because of how reproducible physiological recordings are from ganglion to ganglion, there does also exist some known anatomical variability. Frequently, the position of somata varies although this is unlikely to impact their connectivity. There are also known cases of cells staining for certain neurostransmitters or receptors varying in number from ganglion to ganglion, suggesting variability exists for the composition of each ganglion (Bratka personal comm., KL Todd personal comm., Lent et al., 1991). It's likely that there will exist some cases in which two cells are synaptically involved in one ganglion and not in another, or reproducible connections that involve differing numbers and locations of synapses. Unfortunately, the high time and labor commitment required to produce full cell reconstructions and annotations currently limits image acquisition and analysis to a single ganglion. In other systems, measuring sample-to-sample variability has thus far been largely confined to two samples. In the earliest connectome, *C. elegans* was reconstructed from partially overlapping datasets from different animals; the connections found in the region of overlap were largely consistent from sample to sample (White et al., 1986). Similarly, Ohyama et al. (2015) found that in the region of overlap between the two volumes they collected, 96% of connections involving two or more synapses in one animal were also found in homologous cells in the other animal. Randel et al. (2015) has also compared connectivity patterns in a partial connectome of *Platynereis* visual system and similarly finds high concordance between two animals. Moving beyond these low N experiments will eventually require even further acceleration of imaging and analysis. In particular, automated and semi-automated reconstruction and annotation

techniques currently in development (Berning et al., 2015; Kasthuri et al., 2015; Helmstaedter 2013) could considerably decrease this time cost, enabling larger sample sizes.

Connectomics seeks to provide rich interpretable datasets to be used in order to develop and test hypotheses governing circuit function. For example, the entire field of *C. elegans* neurobiology relies, to some extent, on the known connectome in order to guide targeted genetic experiments and recordings (Bargmann and Marder, 2013). The level of detail achievable with connectomics enables discoveries like the localization of synapses among direction-selective retinal ganglion cells and starburst amacrine cells (Briggman et al., 2011). Even in systems with a high degree of genetic typology like the mouse retina, new cell types have been reported on the basis of connectomic analysis (Helmstaedter et al., 2013). Similarly, connectomics has been used to reveal new cells involved in known pathways in the *Drosophila* visual system (Takemura et al., 2013). Connectomics is thus enhanced by unifying its findings with physiological recordings (see also Bock et al., 2011).

Along these lines, our results demonstrate the utility of applying serial EM reconstruction to a system in which individual neurons can be identified from preparation to preparation. Known connections can be verified or challenged, and previously unknown connections can be discovered and subsequently tested. This connectomics approach enables the interplay between anatomical thoroughness and physiological precision that will allow future researchers to uncover previously inaccessible details regarding the circuits underpinning behavior in the leech ganglion.

Chapter 3 represents work being prepared for publication. Jason Pipkin, Eric Bushong, Mark Ellisman, William Kristan. The dissertation author was the primary investigator and author of this material.

Chapter 4. Conclusions.

In this thesis I have presented data from the first large serial EM volumes spanning portions of the leech ganglion. In Chapter 2, I discuss anatomical features observed within these datasets, focusing in particular on the presence and type of vesicles within arbors and on the coarse spatial distribution of synaptic input and output sites. In Chapter 3, I show that full reconstructions of arbors belonging to identifiable neurons can be used to confirm, challenge, and predict synaptic connections among them. In sum, these data serve to demonstrate the utility of applying SBEM to the physiologically accessible, robust, and reliable leech ganglion. This thesis lays the ground work for further connectomic analysis of the leech nervous system. What will go into that work – and what could come from it? In this final chapter of concluding remarks and discussion, I briefly consider the challenges and future of connectomics as a field.

Challenges of connectomics

Connectomes, even partial ones, contain immense value in their precision and completeness. In a volume of serial EM images, every neuron, branch, and synapse is contained, waiting to be counted and labeled. No other approach affords that level of detail at that scale. Given this power, connectomics can sometimes be promoted with an aura of deterministic grandeur. When Sydney Brenner's group published the connectome of *C. elegans*, their article was subtitled "The Mind of the Worm" (White et al., 1986). Sebastian Seung popularized connectomics to the public with a Ted Talk entitled "I am my connectome" (Seung, 2010 available at: https://www.ted.com/talks/sebastian_seung). Recently, The New York Times has covered connectomics from the perspective of feasibly

reconstructing and uploading cryogenically frozen minds (Harmon, 2015 available at: http://www.nytimes.com/2015/09/13/us/cancer-immortality-cryogenics.html).

Of course, a connectome is not all there is to know about a person, animal, or ganglion (as John White, Sebastian Seung, or Amy Harmon would freely admit). By analogy to a connectome, consider Renoir's *La dejeuner des canotiers* (1881) (Figure 1). An impression is formed of an ensemble of individuals whose positioning and gazes reveal the relationships among them. Of course these characterizations might not even be that accurate ("Is that a look of longing and desire or bitterness and apathy?") and the image is fixed in time – the viewer can only infer what has occurred or what might occur. Finally, one can't experimentally perturb a painting – what would happen if one person left the party?

Figure 1. **Renoir, *La dejeuner des canotiers***. 1881. The impressions formed of individuals and their relationships in this painting is analogous to those formed of neurons and their connections in a serial EM dataset (see text).

Connectomes similarly offer only a fixed view of a highly dynamic system. While we can ascertain neuronal anatomy and connectivity from a serial EM volume, we often cannot

know for certain how strong a given synapse is, or, in many cases, whether it's excitatory or inhibitory. Connectomes contain information about the presence of large neurosecretory vesicles but not necessarily enough to be able to determine where they're released or the radius of their effects. In this section I consider various challenges and drawbacks to connectomics and discuss whether or how they are being or can be addressed.

Determining neurotransmitter identity – From a series of EM images, is it possible to determine whether a given synapse is glutamatergic or GABAergic? Dopaminergic or serotonergic? Part of the motivation behind describing the vesicular content of neuronal arbors in the leech (Chapter 2) was to explore whether it was possible to ascribe neurochemical identity on the basis of observable anatomical features. In our case, this was largely unsuccessful. There were a lot of patterns: neurons with boutons full of vesicles and neurons with multiple small vesicle fields in a given bouton; neurons that contained vesicle fields in their primary branches and those that did not; neurons that contained vesicles only within one half of the ganglion and neurons that contained them throughout their arbors; neurons with aggregations of larger vesicles at their presynaptic boutons and neurons that had vesicles of the same appearance aggregated only within their somata and individually scattered throughout their branches.

In only one case however did we feel confident identifying large intensely-staining dark vesicles as serotonergic. The features that led to this limited finding are informative. First, we had a very obvious phenotype: these vesicles stained so intensely that they were easily identifiable. Second, we had a lot of previous research to indicate that dense-core vesicles (which stain more intensely, hence "dense") could be serotonergic (e.g. Muller, 1979; Kuffler et al., 1987, Trueta et al., 2012). Thirdly, we had a known pattern of

serotonergic neurons (Lent et al., 1991) that matched the dark vesicle-containing somata in our juvenile ganglion volume. In this case, strong prior knowledge enabled pattern matching with a readily identifiable phenotype. This same approach has been taken by others. In order to identify synapses in the retina in a dataset that contained no intracellular staining and therefore no vesicles, Briggman et al. (2011) relied on known characteristics of GABAergic starburst amacrine cell synapses in order to identify connections.

It remains to be seen how generalizable this "pattern matching" approach is. For now, there likely remains some fruit on the lower branches. In studies using higher resolution TEM, previous work has been able to discriminate different classes of small vesicles on features like granularity and size (Muller and McMahan, 1976; King 1976; Kilman and Marder, 1996). Therefore some information is present within the tissue that is simply waiting to be revealed by improvements to imaging technologies that enable the resolution required to discern it. There is also potentially informative classifying patterns in higher-level structural details like branching pattern, order, angle, length and so forth. Ultimately, however, it is worth considering when it is even necessary to find anatomical correlates of neurochemistry. Certainly in the case of the leech it is perhaps more straightforward to identify a cell by its soma position and arbor shape and subsequently use a combination of physiology, histochemistry, or even single-cell transcriptomics in order to determine which neurotransmitters it releases. Even in the case of the mammalian cortex, many cell types have known neurotransmitter phenotypes that correlate with their physiology, anatomy, and location (e.g. GABAergic interneurons in the hippocampus [Klausberger, 2009]). As far as connectomics is concerned, correlating these features with ultrastructural information is

perhaps most useful when analyzing volumes that do not contain the full arbor of every neuron present.

Determining synaptic strength – From a reconstruction of two synaptically involved cells in a serial EM volume, is it possible to predict how a spike in the presynaptic cell will influence the postsynaptic cell? If connectomics is to produce useful contributions towards understanding the function of nervous systems, it must be able to inform models that seek to explain just that. Determining synaptic strength involves at least two parameters: (1) how strong a given synapse is, and (2) how many synapses there are and where they're located. Determining the first from anatomical data seems out of reach. Theoretically, being able to do this would involve some combination of the following tasks: resolve the number (and molecular composition) of postsynaptic receptors, the area of the active zone, the precise shape of the synaptic cleft (in order to model diffusion), the presence and molecular identity of proteins that break down or recycle neurotransmitters, an estimate of release probability (realistically, a model that accounts for temporal dynamics), and basically everything else that goes into the complex machinery of an individual synapse. Some of these might be achievable with higher resolution imaging or selective protein tagging, but for now most efforts seem to concentrate on the second parameter listed above: how many synapses are there and where are they located?

In Chapter 2, we showed that certain leech neurons possess synaptic outputs only in half of their arbors and that others lacked any chemical synaptic outputs (at least within the neuropil of the ganglion). In Chapter 3, we showed that the synapses between cells known to be synaptically involved were numerous (though this number varied) and widely distributed, contradicting previous work (Lytton and Kristan, 1989). Had I had another thesis

and a dataset of more uniform quality, it would have been interesting to see whether known variability in synaptic strengths (e.g. among the P cells and cell 212; Lockery et al., 1990) correlated with variability in synapse number. In one case in the nematode *Ascaris suum*, morphological synapse number did not correlate with synapse strength (Angstadt et al., 2001).

For many systems and synapses, number might not be as important as location. We frequently observed synapses from one presynaptic bouton onto another (the S cell was a notable participant in these arrangements) and these "serial synapses" have been observed in invertebrates before (Muller and McMahan, 1976; Graubard, 1978). For invertebrates with monopolar neurons, synapse location presents an unusual challenge given that the spike initiation zone (or zones) are not readily identifiable anatomically the way an axon hillock of a vertebrate pyramidal cell is. Being able to identify these, perhaps with the aid of a molecular tag, is a key challenge particularly if one wants to build a detailed model of cellular function.

Neuromodulators and medium- to long-range signaling – How can one tell where exactly and in what number neuromodulators are released from neurosecretory granules? How far do they diffuse? Where are receptors for them located on postsynaptic cells? Neuromodulators are known to have profound impacts on the function of known circuitry. For instance, in *C. elegans* neuropeptides can alter which cells are recruited into a sensory circuit (Leinwand and Chalasani, 2012). In the crustacean stomatogastric system, a plethora of neuromodulators can impact the state of its ongoing rhythms (Marder, 2012). Notably, both of these systems have "known" connectomes (White et al., 1986; Marder, 2012).

The leech – along with probably every nervous system – is also subject to neuromodulation (the Retzius cells are even known to release serotonin from their somata [Trueta et al., 2012]). Is it possible to predict the effects of neuromodulators from anatomy? In Chapter 2, we showed that large vesicles, whether serotonergic or very large and clear, are present in both aggregations and individually in some arbors. The aggregations and synaptic boutons seem telling: why would there be so many there if they weren't also released there? On the other hand, the presence of scattered individual vesicles throughout arbors, including branches that don't contain presynaptic boutons, suggests that these vesicles might be releasable almost anywhere. Indeed, there is likely no simple anatomical evidence by which a serial EM dataset can ever reliably predict where, what, and with what efficacy neuromodulators influence the neighboring synapses and arbors.

Dynamics – How is it possible to predict the changes of synaptic strength or even the shapes of the neuronal arbors themselves from a serial EM volume? Synapses undeniably change over time, and these changes can be structural (Baily and Chen, 1991; Wilke et al., 2013). Given a single serial EM volume, studying (or predicting) dynamics is impossible. However, it is at least theoretically possible to imagine a future in which the time and effort costs of generating these volumes have shrunk low enough to the point that collecting multiple volumes of a given brain region from many individuals at different time points could be possible. For now, inferring dynamics from a single snapshot is not possible – a connectome generated by a single volume must be paired with pre-existing models of both cellular and synaptic dynamics before it can be used to most accurately model circuit function.

The future of connectomics

The principle appeal of connectomics is that part of what makes an animal feel, think, and do what it does is the precise connectivity pattern of that animal's nervous system. But given the challenges listed above, it is appropriate to ask to what extent that wiring diagram matters. How much do the connections among a set of neurons constrain the activity patterns those neurons can generate? While I cannot answer this fundamental question here, I think it is worth reflecting briefly on how useful connectomes are and will be even in light of their limitations.

To start with, the *C. elegans* connectome has been available since 1986 (White et al., 1986). And while every *C. elegans* neurobiology talk I've ever attended has emphasized the fact that "they still don't know how it works" somewhere during the first few slides in order to motivate their work, most allow that it has proven invaluable. Within the *C. elegans* community, the connectome is used as a guide for experiments. For example, Leinwand and Chalasani (2012) knew to record from one of the interneurons in their work because they knew it received inputs from the sensory neurons they were studying. Indeed, the experiments that revealed the function of many sensory neurons in *C. elegans* were designed on the basis of the connectome (Bargmann and Marder, 2013).

As noted in Chapter 3, connectomes have been used to discover completely new synapses (in our case between the S cell and cells 116) and circuits (Takemura et al., 2013; Randel et al., 2014; Ohyama et al., 2015). In addition to the connectivity information, connectomes also can faithfully reproduce the structures of the neurons they contain. Combined with connectivity, this structural information can prove very useful for classifying

neurons, as Helmstaedter et al. (2013) demonstrated by discovering a potentially new bipolar cell in the mouse retina.

Connectomes, as they exist today, are most useful when paired with a physiologically or genetically pliable system in which connectivity predictions can be tested. This is the case with cell-specific ablation or calcium imaging in *C. elgans* (Leinwand and Chalasani, 2012; Bargmann and Marder 2013) and *Drosophila* (Ohyama et al., 2015), or cell-specific electrophysiology as demonstrated in the leech ganglion in Chapter 3. Importantly, the ability to test an anatomical feature physiologically depends on how reliably that feature is found from preparation to preparation. Testing if a connection exists at all is the easiest experiment. But what about correlating synaptic strength (measured across multiple individuals) relative to synapse number (measured in one serial EM dataset)? It's certainly possible that natural variability could produce wide swings in something like synapse number in the same way that intracellular dynamics can vary from preparation to preparation in the crab stomatogastric ganglion (Goaillard et al., 2009). Addressing this issue simply requires that imaging and analysis of serial EM volumes be reduced in time so that multiple samples can be collected. Practically, this means that if, for example, experiments are ongoing to map an entire larval zebrafish brain or an entire *Drosophila* brain then it is technologically feasible and scientifically worthwhile to collect additional *C. elegans* samples.

Concluding remarks

In the end, the strengths and weaknesses of connectomics highlight two important truths about neuroscience in general. First, knowing one parameter (like connectivity) does not solve the jigsaw puzzle. Multiple approaches must be made to work together. In the leech, these are connectomics, electrophysiology, and voltage-sensitive dye recording. In the

fly and worm, these are connectomics, genetics, and calcium imaging. Second, individual variability is a feature of nervous systems. There is a tendency to talk about "the" connectome of the worm, or to speculate about "the" mouse connectome. Yet connectomes are almost certain to vary between individuals – and how they vary is probably their most interesting feature anyway. Connectomics therefore has the potential to shift how the goals of neuroscience are perceived in general. In light of the detail and potential variability that connectomics reveals, "How does the brain work?" will become an increasingly insufficient question relative to "How does any given brain work?" Addressing this question will require an experimental preparation in which it is possible to combine physiological precision with anatomical detail. The progress presented in this dissertation demonstrates that the leech ganglion can be such a system.

Appendix A. Parameters and challenges of data acquisition.

While on the microscope, the acquisition of serial blockface scanning electron microscopy (SBEM) datasets is relatively fast, easy, and straightforward. During my thesis work, we collected four "volumes" of serial images. The first volume of adult neuropil (96µm x 96µm x 17.3µm) was collected on an FEI Quanta FEG SEM equipped with a Gatan 3VIEW SBEM system during an imaging run that lasted a day and half. By the last volume, using the newer Zeiss MERLIN system with a Gatan microtome we were able to collect images spanning an entire juvenile ganglion (~225µm x 225µm x 136µm)) in six weeks. Achieving these data acquisition rates and maintaining image quality involves the tricky balance of a number of variables. And even with the most optimal set of variables, inevitable problems will arise. In the following two sections, I discuss in detail the parameters needed to produce quality images of large volumes in a reasonable amount of time and I elaborate on every imaging-related problem that I encountered. As there exists another laboratory now attempting to gather an even larger volume of leech tissue, I hope that the following discussion can be of value to them as they prepare for image acquisition.

Imaging Parameters

The goal in serial EM is to produce a volume of tissue a well-aligned stack of images within which it is possible to completely segment any given neuronal process that travels through that volume. Below, I list some (but not all) of the many parameters that can influence image quality throughout the volume.

(1) Staining quality. As with any electron microscopy, "the gain in the brain is mostly in the stain" (quote attributed to Stanley Yolles in Bloom, 1992). Improving the staining quality improves the natural contrast of ultrastructural features like plasma membranes and

mitochondria to the cytoplasm and extracellular spaces. This effectively reduces imaging time by increasing natural signal-to-noise. For leech tissue, improving staining means improving how evenly the various metal stains penetrate into the center of the dense neuropil. We found that it was necessary to briefly microwave the sample while incubating it with osmium stains in order to achieve acceptable penetration (Appendix C). Other protocols developed to improve stain penetration in the mouse brain are now emerging that employ different staining chemistries, and may be worth exploring in invertebrate preparations as well (Mikula and Denk, 2015; Hua et al., 2015).

(2) Dwell time. Current SBEM machines create images by scanning the electron over the sample pixel by pixel while recording backscattered electrons. Dwell time is how long the beam lingers on a region of the sample that will become a single pixel. In current systems, dwell time can be as fast as 0.5 µs and efforts are always underway to reduce this further. If reducing imaging time is a major concern, then reducing dwell time is a critical variable. On the other hand, longer dwell times improve signal to noise (averaging backscattered electrons over a longer period of time). I found that a dwell time of 1.0 – 1.5 µs produced the best quality images when sampling the juvenile ganglion volume (the adult ganglion neuropil was imaged at 8.0 µs dwell time). However, if dwell time is too high, then depending on the beam voltage the electron dose may be enough to render the surface of the block too soft to cut cleanly.

(3) Magnification and raster size. Magnification controls the area of the sample being imaged (a higher magnification means a smaller area is imaged) while raster size controls how many pixels are imaged within that area and therefore the size of the pixels. Together, both these variables produce resolution, typically measured in pixel size. It is

important to note that image quality – a subjective impression – is not necessarily linked to pixel size. I have found that magnification is typically more important than raster size and would almost always recommend montaging multiple tiles at higher magnification and lower raster size rather than taking a single image at a lower magnification and higher raster size, even if pixel size is comparable between the two approaches. Effectively, I found that a given pixel size produces better looking images when magnification is higher. However, with high enough signal-to-noise, it may still be possible to get a very good image at lower magnification and avoid having to montage as much, which does reduce total imaging time.

(4) Cutting thickness. This determines how much the ultramicrotome slices off after each image is taken of the block surface. Effectively, this is the z-resolution, although keep in mind that the real z-resolution per image is determined by from how deep within the sample backscattered electrons are produced and detected (Denk and Horstmann, 2004). For this variable, it is important to select a thickness that is at most half the thickness of the thinnest cellular feature that one is interested in segmenting. For neuronal processes in the adult leech ganglion, that means a cutting thickness of 35 – 40 nm is ideal, although I found I lost very few processes due to section thickness even in our volume of adult ganglion neuropil that was cut at 70 nm. For time considerations, thinner sections increase the overall time. For image quality considerations, thinner sections typically means that dwell time must be reduced in order to eliminate the possibility that the surface of the block will become soft under the beam and not cut cleanly.

(5) Montage overlap. When montaging, or taking multiple tiled images of the block surface, the overlap determines how much each tile overlaps with its neighbors. The generic advice is to have at least 10% overlap. While it is possible to get away with less and

therefore decrease imaging time, I don't recommend this as it might necessitate manual reconstruction of the montages if the automated algorithms don't have enough information to work with. Also it is important to note that the overlapping portions of each tile receive twice the electron dose, and therefore caution must be taken to ensure that this doesn't result in cutting artifacts.

(6) Run length. The time during which the machine is imaging and sectioning is the "run". For long overall runs, I recommend using several short runs instead. This allows the experimenter a natural time to readjust focus and reposition the area being imaged if necessary.

Potential Imaging Issues

During my experience with SBEM I have become quite acquainted with the wide variety of things that can go wrong. In some cases these were expected, in others completely unexpected. In the interest of passing this wisdom on so that others may avoid these issues, I list everything that went wrong below.

(1) Areas of damaged or poorly-stained tissue. Even in an otherwise well-stained and well-preserved sample, it is possible to have some areas in which the tissue appears damaged or does not stain well. As far as staining goes, it is always worthwhile to explore better ways to get more contrast and to do so evenly throughout the sample. It is also important to know that almost everyone doing connectomics is at some point or the other running into patches that are poorly stained, and that this probability increases with the size of the imaged volume.

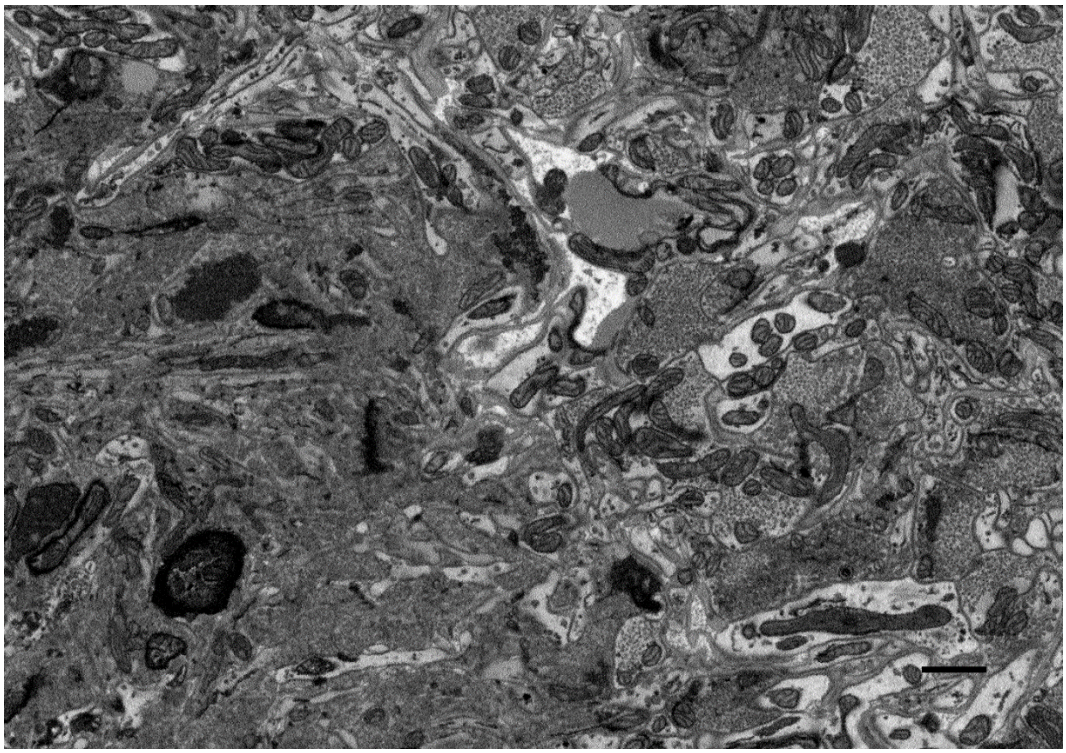

Figure 1. Poorly stained neuropil. A region of poorly stained low-contrast neuropil (left half of image) adjacent to an area of well-stained high contrast neuropil (right half of image). It is unclear what causes such differences in staining quality. Regions like these underscore the need to thoroughly review staining quality in a test sample before collecting a larger run (though these may occur regardless). Scale bar = 1000nm.

(2) Focus drift. While this problem is largely minimized with current systems like the MERLIN, it is still possible that, over time, the sample may drift out of focus. This can be combatted both manually, by periodically checking in with the run and refocusing, or by employing an auto-focus routine that focuses before each image is taken.

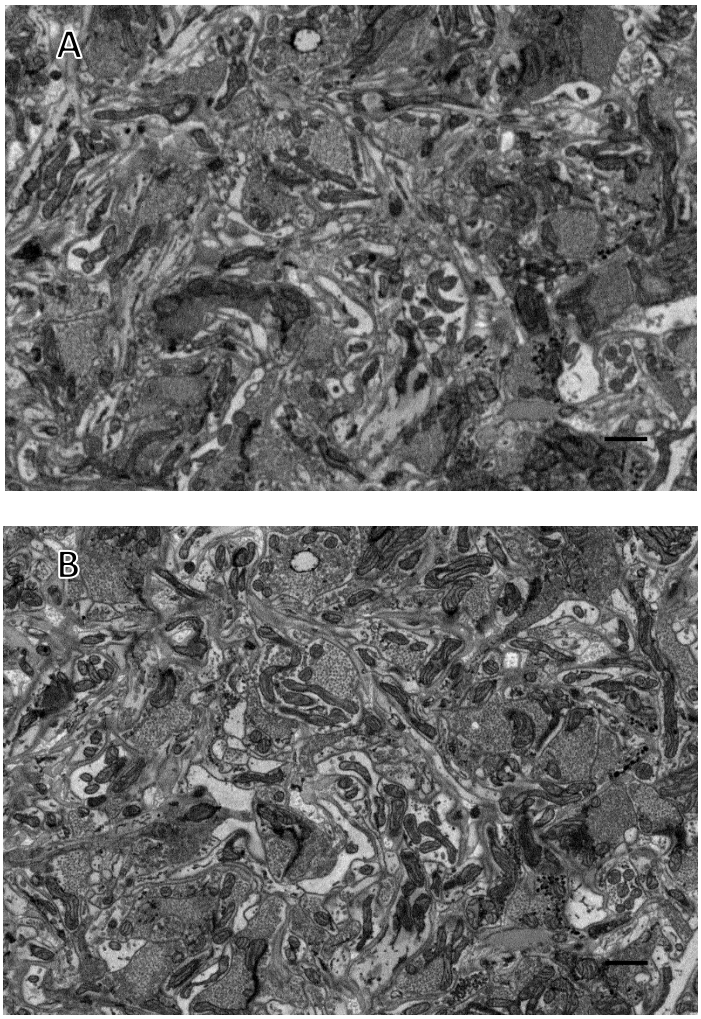

Figure 2. Focus drift. Focus drift over time can result in harder to trace areas. **(A)** The top image is an image of adult neuropil after focus drift. **(B)** The bottom image is the next section of the same area of neuropil after focus was corrected. Scale bars 1000 nm.

(3) Image distortion. Due to how the beam is directed at the sample, sometimes with a wide field of view it is possible to get a distortion effects near the edges of the image. This may also occur even at smaller fields of view to a lesser extent, as I experienced. When producing a montage, any distortion at the edges can make subsequent montage reconstruction more difficult than it otherwise would be.

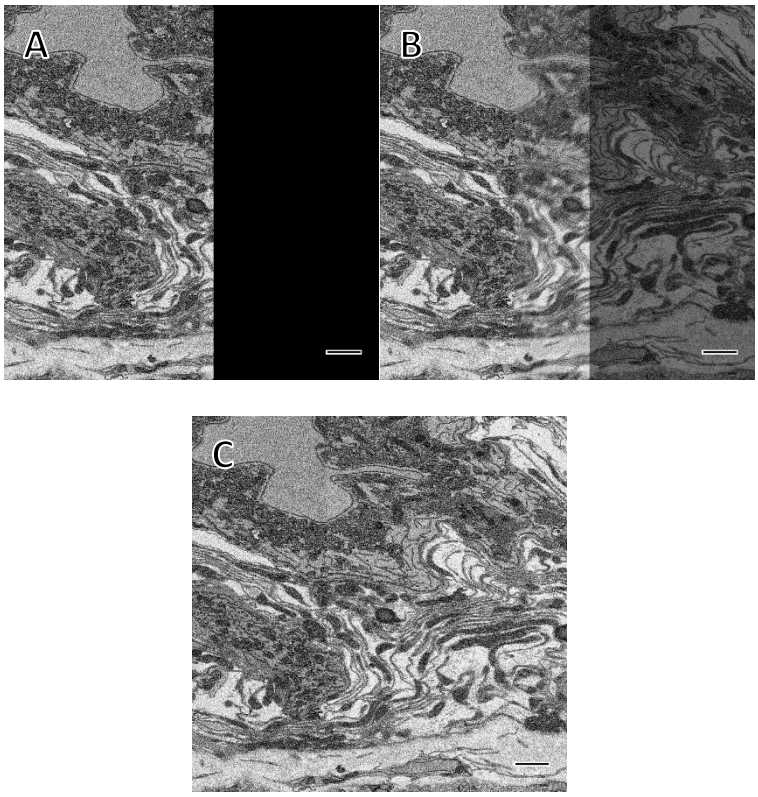

Figure 3. Edge distortion. Edges of images can be distorted. This is noticeable when comparing where two tiles overlap; if the tiles were perfectly flat and undistorted, they would overlay each other perfectly. **(A)** Left tile only. **(B)** Left and right tiles, right tile is set to 50% transparent and overlap region is visibly blurrier due to edge distortion. **(C)** Both left and right tiles at maximum opacity; here the right tile entirely overlays the left tile and only a slight border is visible. Scale bars are 1000nm.

(4) Missing sections. The MERLIN system is controlled by two software programs. One, written by Zeiss, controls and monitors the microscope chamber, beam, and other hardware. The other, written by Gatan, controls the microtome and also interfaces with the detector and the beam. It turns out that it is possible for the Zeiss system to detect (perhaps falsely) that the pressure within the chamber is increasing, indicative of a vacuum failure. Therefore, the Zeiss system will blank the beam. While this is happening, the Gatan software continues happily sectioning and imaging static. While the Gatan software will detect, after a few sections, that the current images are statistically far noisier relative to the previous

images and pause the run, that still means that three or more images are lost and that time is lost while the experimenter needs to restart the run (and this does happen at 3 A.M.). There may be other ways in which sections are lost as well in SBEM that I have yet to encounter (serial TEM work is notorious for being vulnerable to section loss – White, in discussing the acquisition of data for the *C. elegans* connectome has relayed the story of how at one point an entire stack of sections was accidentally dropped down the column of the microscope available at https://www.youtube.com/watch?v=cTQvsJg9cP0).

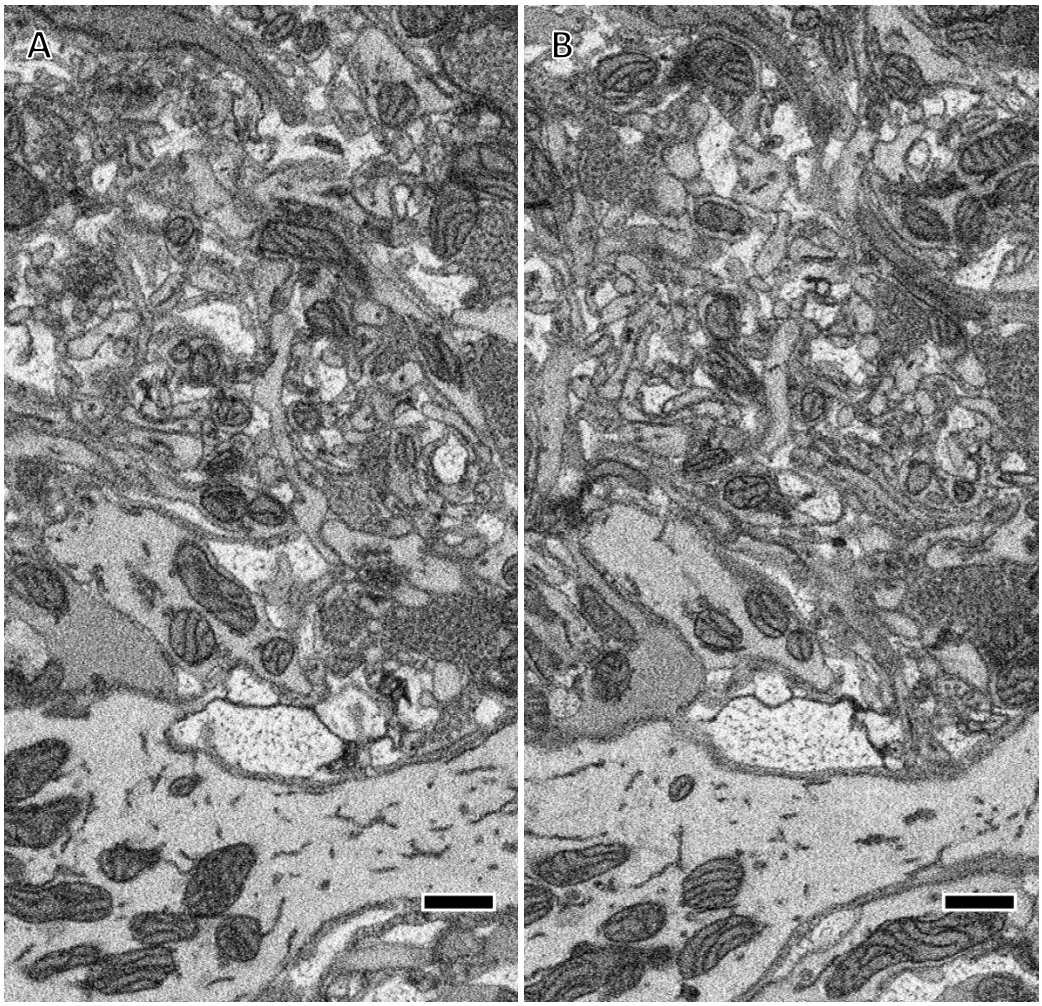

Figure 4. Missing sections. Missing sections produce discontinuities that are difficult to trace. **(A)** Area of juvenile neuropil before missing section. **(B)** Same region after 5 missed 50nm sections. Note that while large features are traceable across the five section gap, smaller features and processes are more difficult to trace.

(5) Cutting artifacts. If the surface of the block gets too soft from a high electron dose, it will not cut properly. This occurred during one run of the juvenile ganglion volume because the Gatan software was incorrectly reporting the dwell time. These essentially ruin the portions of the image affected, and should be avoided at all costs.

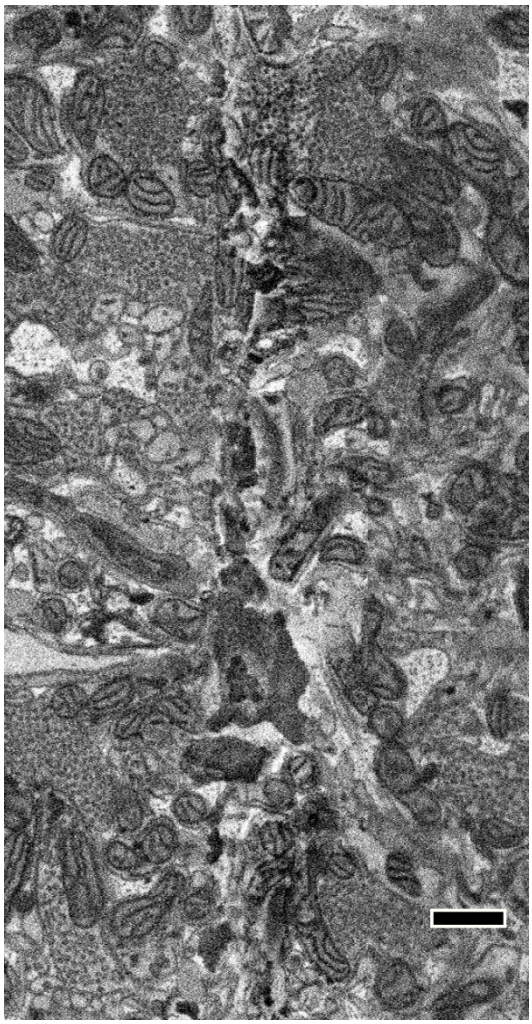

Figure 5. Cutting artifacts. Cutting artifacts are caused by softness in the plastic block. Here, a region of overlap between two tiles was softened due to dwell time being too long. Neighboring regions are unaffected as they only experienced half the beam dose. Scale bar 500nm.

(6) Cutting debris. This is a minor issue. Sometimes a piece of an old section that was left on the top of the knife will fall back off onto the block surface and obscure some

portion of the tissue. This is probably guaranteed to occur occasionally, particularly with a large run, but even then it is not a major problem.

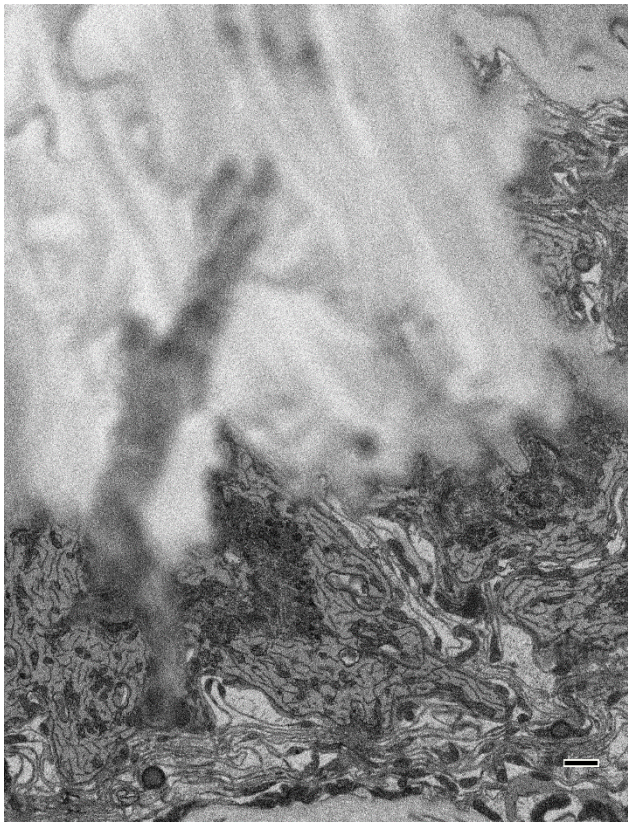

Figure 6. Cutting debris. Cutting debris can occasionally fall off the knife and can obscure underlying tissue. These occur rarely and are always removed by the next section. Scale bar 1000nm.

(7) Charging. As electrons enter the sample from the beam they need a path to reach ground. This path typically goes from the tissue to the edge or bottom of the block where it is then carried to the metal pin upon which the block sits. If there's an area devoid of tissue that's sufficiently large enough that electrons can't escape, they will pool in the plastic there and then effectively act as an electron dense area that can produce backscattered electrons. Worse, these areas can become so dense that they warp the image nearby. For the leech this is only a problem on the edge of the ganglion, and can be

mitigated by very precise trimming. For vertebrate systems, this crops up within nuclei and blood vessels, and is mitigated chiefly by reducing the beam voltage.

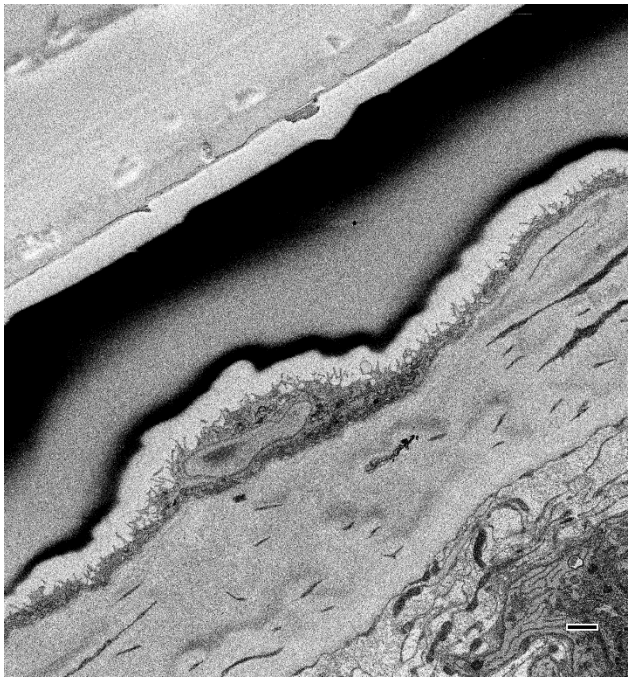

Figure 7. Charging. Charging occurs when electrons accumulate in empty regions of plastic. Here charging is visible as the extreme black band of plastic near the edge of the block. Note that the region near the edge of the block and the edge of the sheath are not charged at all. This is because there are paths through the gold palladium coating (near the edge) and the tissue (near the sheath) that can conduct electrons to the mounting pin under the block. Scale bar 1000nm.

(8) Unexpected loss of contrast. In the juvenile ganglion run, images became progressively less and less contrasted as the run continued. This, it turns out, was due to the filament on the electron gun wearing out sooner than it was supposed to (a problem in turn due to the maintenance contractors using the wrong replacement filament). This kind of problem is avoidable now that it is known, but was unavoidable (and indeed unknown) at the time. It is certainly possible that, in the future, other unknown unknowns could crop up to ruin a run.

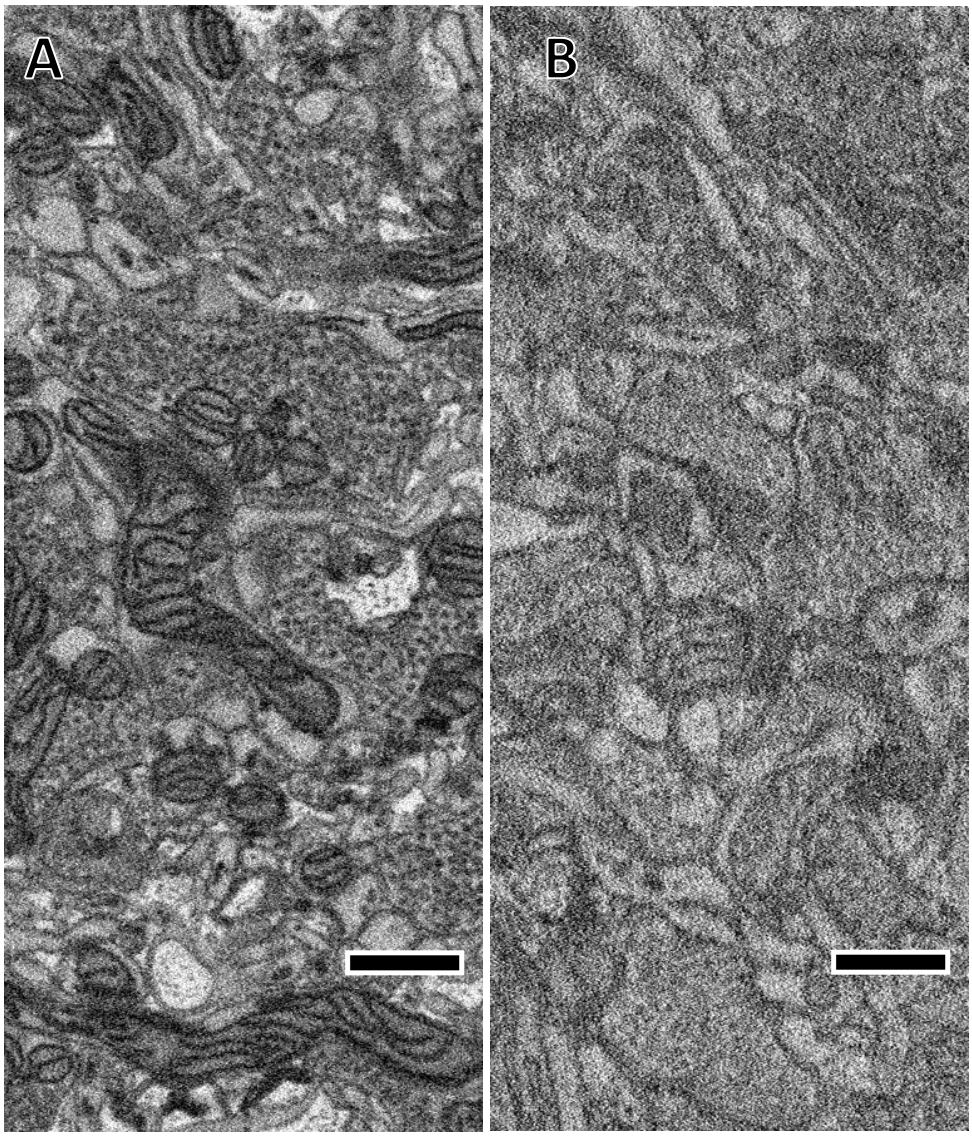

Figure 8. Contrast loss. In the juvenile ganglion dataset, we experienced an unexpected gradual degradation in contrast. **(A)** A region of neuropil near the beginning of data acquisition, in the dorsal half of the ganglion. **(B)** A region of neuropil near the end of data acquisition, in the ventral half of the ganglion. The poor contrast region is not entirely untraceable, but it is noticeably more difficult. Scale bars 500nm.

(9) Uneven focus from tile to tile in a montage. One issue I found as I reconstructed the volume of images spanning the juvenile ganglion is that tiles at the periphery of the 5x5 montage were occasionally slightly out of focus relative to tiles at the center. When focusing, I always focused on the center, as one is required to center the sample within the

montaged field prior to imaging. To avoid this problem in the future, I recommend using an auto-focus feature per tile, or simply reducing the number of tiles. Note that if using auto-focus on edge tiles of a leech ganglion, it will be necessary to make sure the area being focused contains tissue and is not empty space.

In sum, pushing a newer technology to its limits (the six-week acquisition of the juvenile ganglion was the longest continuous acquisition for NCMIR's MERLIN system) inevitably produces a lesson in learning to accept the good enough when the perfect isn't always possible. Even with everything that can and will go wrong, SBEM produces amazing datasets that are rich enough that a few problems will do little to reduce the overall value of the data. The future researcher would still, of course, be well-advised to avoid any issues, and hopefully my experiences can inform their efforts.

Appendix B. Challenges in analysis of large volumes of serial EM data.

Generating datasets with serial electron microscopy is a time-consuming process fraught with technical peril. Yet analyzing these vast datasets invariably takes far longer. This has been true since the beginning of connectomics. The first attempt to use this serial electron microscopy to map out every neuronal connection in an animal was performed by Sydney Brenner's group in the 1970s and early 1980s (White et al., 1986). They painstakingly sliced over 8000 thin sections (50nm) of the nematode *C. elegans* until, with a few specimens, they had enough sections to represent the entire animal. These were then imaged with a transmission electron microscope. This laborious process – far more intensive than any current approach in connectomics – still pales in comparison to the effort they put in to trace and annotate the resulting dataset. Here they had the idea to use a computer – the approach used today – yet found that even after literally inventing an operating system, text editor, graphics drivers, and a digitizing input system to transfer data from electron micrographs to the computer the power of the system was simply too low (it had only 64 Kb of memory) to do anything other than display parallel bundles of fibers in the ventral nerve cord. The remaining mapping had to be done by manually tracing. This task largely fell to Eileen Southgate, an expert technician, who marked the inside of a process on each print with a special ink pen that could be erased with alcohol. With pen and paper she then noted where each synapse occurred (Emmons, 2015). She repeated this protocol for each process until every neuron had been fully traced – from its inception to its conclusion in 1984, the project took 15 years (Emmons 2015). (The paper wasn't published for another two years as the Royal Society needed to locate additional funding to publish a work that ran some 350 pages over their limit [Emmons, 2015]).

Since their work, novel imaging approaches in both scanning and transmission electron microscopy have dramatically decreased the time required to generate serial EM datasets (Denk and Horstmann, 2004; Knott et al., 2010; Kasthuri et al., 2015). Yet the inevitable requirement for some form of human tracing and annotation continues to be a time-consuming hurdle (Wanner et al., 2015). In addition to its labor-intensive nature, tracing and annotation is inherently error-prone. This section details approaches and techniques in human annotation with a particular emphasis on reducing analysis time and error rate. I particularly compare and contrast the two predominant forms of tracing: full volume reconstruction (creating a digital outline of the plasma membrane of each process in each section) and skeletonizing (placing a single dot, or node, within each process that is automatically linked to the previous node).

Volume Reconstruction

Full volume reconstructions of serial EM datasets involve manually tracing the contour of each cell's plasma membrane in a given section and repeating this throughout the entire volume of acquired data. In this way, one recreates a 3D model of the traced arbor which can then be viewed independently of the surrounding neuropil: a kind of manually-generated Golgi stain. More powerfully than any stain, this can then be repeated for as many arbors as are present in a given sample, allowing researchers to compare the shapes and sizes of various structures. For instance, Wilke et al. (2013) use volume reconstruction to highlight the structural diversity of dendritic spine heads and axon terminals in the hippocampal mossy fiber pathway. Others have employed this technique to exhaustively reconstruct every arbor within a given small volume, then used the resulting data as a basis to answer questions about the basic numbers of axons, dendrites, spines, glial cells, vesicles,

and other features (for examples of dense volume reconstruction see Kinney et al., 2013; Takemura et al., 2013; Kasthuri et al., 2015).

In my work, I used volume reconstruction exclusively when exploring the first volume of adult ganglion neuropil we collected (presented in Chapter 2). After several years of experience, I have learned quite a bit with regards to the benefits and challenges of undertaking such an approach. Tracing the outline of a neural process is not cognitively demanding: one places a cursor on the membrane then clicks and drags the cursor to generate a digital contour that overlays the real membrane. Yet performing this task well reveals many important drawbacks, which I discuss below.

(1) Tracing a membrane over several sections is unavoidably tedious and frequently boring while simultaneously taxing attentional resources as the tracer must be alert to any branch points. A tracer is served well by deep reserves of patience, perseverance, and attention span. In the initial rush to explore the data, this can be easy to attain. My record day was 14 hours of tracing. (I do not recommend spending this much time – I actually saw neuropil when I shut my eyes after tracing too much). Sustaining motivation amongst a team of tracers is certain to be difficult. Most labs have attempted to distribute this task across as many people as possible by employing paid squads of undergraduates (Helmstaedter et al., 2013), or by developing games to induce voluntary participation by citizen scientists (EyeWire – Kim et al., 2014; Brainflight – Helmstaedter 2013), or by inviting scientists in many laboratories to collaborate on tracing (Ohyama et al., 2015).

(2) The most rewarding aspect of serial EM data is the ability to scroll through it: one gets the sense of watching a flipbook animation moving across the screen. Yet tracing the contour of a membrane removes this sense of motion as the tracer must focus on the 2D

image in front of them, scrolling up and down occasionally to confirm a branch point. I emphasize this because I believe that the "flow" of an arbor is an underappreciated (or at least unreported) source of information for the tracer. This is particularly evident to novices: if you show a single still image of neuropil to someone unfamiliar with electron microscopy they will struggle to correctly segment the image. If you then play a movie scrolling through several serial sections those same novices will suddenly and intuitively grasp what they didn't understand earlier as now a field of coherent moving objects. At the very least, they will be able to pick out a few processes and follow them with ease. The facility with which humans can identify that coherently moving pixels belong to the same object is both obvious and remarkable (one is reminded of the random dot task used to investigate visual motion discrimination [Britten et al., 1996]). I speculate incorporating an algorithm that mimics this ability might enhance the reliability of current computer-based automatic reconstruction techniques.

(3) As mentioned in (2), contouring involves spending a lot of time per section. The benefit of this approach is that fewer branches are missed than while skeletonizing (generally, the more time spent tracing an object reduces errors of omission). The cost is that the tracer loses a sense of "flow" and may have to frequently scroll up and down. It also means that a great deal of the work cycle is spent on the physical task of tracing the membrane. For expert human tracers, this is the hugest source of frustration and boredom. I can tell, often at a glance, what the contour of a plasma membrane should be. In fact by scrolling through a series at high speed I can "eyeball trace" what would take me many hours to physically trace.

(4) One must develop a reliable and easy-to-use system for marking branch points to return to for future tracing. As a tracer goes, the process will inevitably branch, sometimes more than once in quick succession with some branches heading "up" in the stack of images and others "down". I quickly discovered that relying on working memory to keep track of all of these is quite impossible and on more than one occasion in my early days of tracing led to me incompletely segmenting an arbor. To some extent this problem is linked to the tracing software being used. In IMOD for instance, there's not a very fast way to leave a digital marker of an unfinished branch and travel back to it later without navigating several menus. While skeletonizing in TrakEM2, on the other hand, it is possible to simply hover over a node and tag it (I used "Unfinished End" as my tag). I then wrote a script that recursively takes me to the nearest unfinished end from where I was in my skeleton in order to finish tracing every branch. Contouring in TrakEM2 would also present the frustration of having to navigate menus in order to leave a marker.

(5) As in (4) one must develop a system for annotation that is fast and reliable. Again, this is a function of software, as having to navigate menus in order to mark the location of a synapse is a frustrating interruption to the tracer's work flow. Tagging nodes in a skeleton is again much simpler.

Volume reconstruction produces stunning images and is clearly useful scientifically given the information it reveals about structural diversity. For some projects, analyzing the three-dimensional structure is and will continue to be the entire purpose. Importantly, all current automated segmentation approaches relies on determining where the plasma membrane is. Therefore as automated segmentation advances, volume reconstructions are

the future of purely connectomics work even in cases where researchers are mainly interested in which neurons synapse with which other neurons and not on their shapes.

Skeleton Reconstruction

As the name implies, “connectomics” is primarily interested in which neurons make synapses with each other. Towards that end, reconstructing the cell is just a means to an end: locating all of that cell’s synaptic partners and identifying who those partners are. With this goal, the three-dimensional structure of the neuron is ultimately unimportant as the data are eventually reduced to a connectogram representing neurons as nodes and synapses as directional lines linking those nodes.

To achieve this result as quickly as possible with manual reconstruction techniques, it is unnecessary to fully trace the outline of the neuron’s plasma membrane in each section. Instead, one can merely place a dot – hereafter referred to as a node – within the bounds of the plasma membrane. Then on the next image slice, another node is placed, and the two are linked by a line. If a branch point occurs resulting in two separate enclosed regions of the cell, two nodes are placed in that section (one within each region) and both of these are separately linked to the previous node. In such a way one builds up a “skeleton” of the neuronal arbor. In the same way that a stick figure captures the essence of the human form, the skeleton represents the neuronal arbor. And even more importantly than revealing a minimalist version of the structure of the cell, the nodes of each skeleton effectively act as coordinates. When a synapse is found, its location is recorded by tagging or otherwise noting a node where that synapse is.

Skeletonizing has been employed throughout connectomics. The *C. elegans* connectome, for example, was reconstructed by marking the inside of each neuronal process

with a letter, then manually recording where synapses occurred (White et al., 1986). Today, software eliminates much of the need for written annotation. Instead it is common to "tag" a node with a short text phrase that signifies something of interest (in my work, I frequently used tags like "unfinished end", "synapse", "vesicles", and "gap junction?"). Nodes can also be tagged in more operational ways, for instance in TrakEM2 it is possible to link two nodes from separate trees with a "connector" object, which is essentially a directional line and, if done exhaustively, allows you to output a connectivity graph directly from the annotated data. Many modern connectomics projects rely on skeleton reconstruction. In the published literature, skeletonization has been employed by Briggman et al. (2011), Bock et al. (2011), Helmstaedter et al. (2013), Mikula and Denk (2015), and Ohyama et al. (2015) among others. I used skeletonization for almost all the tracing done with the juvenile volume, in which whole cells were traced and synapses between them identified. As I did with volume reconstruction, I discuss below a list of several caveats that anyone attempting or possible reviewing work involving skeletonization should be aware of.

(1) Skeletonization is faster, but less time spent on a given section means that the risk of missing a branch point is higher. As discussed in item (3) in the Volume Reconstruction section above, spending a lot of time tracing the contour of a cell membrane makes it very difficult that, when transitioning to the next slice, a branch point will be missed. When skeletonizing, one is often just clicking on a mitochondrion or cytoskeletal structure near the center of the contour. Like a driver on a long road trip just mindlessly focusing on staying in their lane, sometimes this means that the tracer can "miss their exit" and fly right by a branch point. Combatting these errors of omission requires careful review

of the skeleton and, in the best case, independent tracing of the same skeleton (see, for example, Helmstaedter et al., [2011]).

(2) While typically quite fast, generating a skeleton can be time-consuming when the neuronal processes is thick, has multiple branch points in a given section, and is traveling parallel to the plane of imaging. While it feels natural to place a single node at the center of a roughly circular cross-section of a neuronal process, doing so for an elongated twisting cross-section that spans tens of microns (as occurred many times in the primary processes of leech neurons) is awkward at best. In many cases, this results in a node in one section being tens of microns away from the branch point in the next section and this produces a skewed view of where that branch originates when viewing the resulting 3D skeleton.

(3) When processes are traveling in the plane of sectioning, they can often swim up and down through a range of slices. This is not a major problem for skeletonizing, but it does produce some artefactual branches. If the process is thick enough, at each point where the arbor turns down or up in the volume a short branch will be created in the skeleton where no branch would exist at all in a full volume reconstruction. One can leave these areas untraced, but doing so risks leaving unlabeled a portion of the neuron which is involved in synaptic activity that one might be interested in knowing about later.

(4) The speed of manual skeletonizing often reveals limitations in the hardware and software used to generate them. As I traced, I frequently wanted to rapidly place a node, advance to the next section, place another node, and repeat. On the hardware side, this requires that the system be able to load a new image effectively instantaneously. This is possible if the images are all preloaded into the computer's random access memory (RAM). However, loading the image from a hard drive inevitably takes some time given the size of

the images involved (even if tricks are employed to load down-scaled versions). This hiccough in time is enough to be livable but very far from optimal. On the software side, the program needs to be capable of adding a node as quickly as one can advance the image. One issue I ran into with TrakEM2 is that even if I had all the images in a range preloaded into RAM, I couldn't quickly go through them and add nodes in rapid succession. These "quality of life" issues for tracers may seem unimportant, but in my opinion as long as tracing remains manual they are absolutely essential to address. Currently, reconstruction efforts are shifting towards hosting the datasets online. This enables many collaborators to work on the same dataset at once, but it also means that each collaborator has to deal with some wait time in order to download the images belonging to a given section from the server each time they want to progress through the volume. Since it is possible to now stream 4K internet video, it should equally be possible to stream a buffer of images from serial EM dataset to a user's computer which the user can then scroll through at will and annotate as quickly as they can click.

Skeleton tracing reveals neuronal structure rapidly and facilitates straightforward annotation of synapses and other features of interest. While volume reconstruction will eventually replace skeleton tracing as automated techniques advance, for current manual tracing projects with connectomic goals, skeletonization is virtually required.

Tracing errors

Whether manually skeletonizing or reconstructing a full volume, errors will occur. These naturally arise from the limits of computer vision or human attention, from ambiguities in the data, from biases inherent to the dataset, or from biases in the mind of the tracer. These produce several kinds of errors which I discuss below.

(1) In volume reconstruction, one might accidentally include excess matter or exclude some portion of the traced neuron. Essentially these are errors in contouring, or in drawing the line following the membrane. In most cases a very little bit of the neuron will be excluded or a very little bit of neighboring material will be included. For most purposes, such tiny mistakes are likely to be negligible. For others (e.g. detailed modeling of the diffusion of particles through the extracellular spaces) they might end up being significant. These small mistakes are easily combatted by reviewing.

(2) Current methods of fixation and eventual dehydration lead to a shrinking of the extracellular space in the neuropil (Hillman and Deutsch, 1978; Korogod et al., 2015). This (and even efforts to counteract it) introduce inherent biases to the precise shape of neurons. Cells might appear to be more swollen than they are *in vivo* which means that any modeling that depends on precisely estimating cell volume or surface area is going to be difficult (though not impossible, see Kinney et al., 2013). The reduction of extracellular space effectively pushes all processes together which, in some cases, could lead to aberrant synapse identification.

(3) Errors of omission, or missing branches, are guaranteed to occur whether doing full volume reconstruction or skeletonization. In my experience and the experience of others (see Ohyama et al., 2015) these are far more common than errors of commission, or attaching a branch belonging to another cell to the traced cell. As discussed above, missing a branch is more likely when skeletonizing versus doing a full volume reconstruction due to differences in time spent per contour. These errors tend to arise due to a lapse in attention that results in either not noticing a branch splitting off or forgetting to label or leave a marker that a branch has occurred and never returning to that area. As one would expect,

experts make fewer of these mistakes than novice tracers. While these mistakes are cleaned up by thorough review and by repeated independent tracings (Helmstaedter et al., 2011), some limits are also imposed by the quality of the dataset. For instance, if the neuron being traced has many small thin branches (<100 nm diameter) that are running in the plane of sectioning, the sections need to be sufficiently thin to follow these processes confidently. Combined with poor image quality, I suspect that this greatly increased the number of missing branches in my tracings in the juvenile ganglion dataset (especially in the ventral portion of that dataset). Also, any missing slice or other break in the dataset is likely to result in traced branches ending prematurely.

(4) Errors of commission, or adding a branch to a given neuron that doesn't belong to it, are far less common. Again, these are far more likely to occur under the hands of novice tracers than experts. They tend to arise in confusing areas with lots of intracellular material that abuts and obscures the path of the plasma membrane. In my experience, I was far more likely to commit these errors before I gained a sense of how arbors moved through the volume and I made these mistakes almost exclusively in the first volume I traced (the adult ganglion neuropil). I know of only one instance where I made such an error in the juvenile volume. This occurred at a break point in the data where three sections were missing. In attempting to trace the process I was in across this gap, I accidentally went into a neighboring process. In this case, I almost immediately began feeling uneasy about the tracing and soon traced the erroneous process back to another nucleus. This highlights an advantage to having large volumes: the more somata and full arbors that are included, the more likely that any given process can be traced back to its parent cell. Yet this also highlights some important limitations: what if the dataset quality is poor enough that not all

process can be traced back to their cell or arbor of origin? Or what if there exist legitimate "orphan" arbor fragments that are essentially unconnected to any cell? It thus remains possible that one can erroneously include certain branches that are short enough and never be aware of the mistake. This possibility naturally increases in a dataset of poor quality, but note that I find orphan arbors in areas of good quality and others have reported orphans in their data as well (Ohyama et al., 2015). Counteracting these errors is again done by careful review or independent tracings. There are also some things that I have learned to keep in mind while tracing. First, it helps to pay attention to the tendencies of the arbor being traced. If it has not included vesicles and then suddenly some appear, it might be worthwhile to immediately double check. Secondly, the thickness of the process tends to be informative. Thinner branches occasionally lead to brief thickenings (especially at a branch point) but more often than not lead to still thinner branches until the branch terminates. Thirdly, it is always worthwhile to leave a note when tracing becomes unsure so that troublesome areas can be more readily reviewed.

(5) Bias can influence synapse annotation and tracing in general. In the ideal tracing arrangement, tracers are blind to the cell they are tracing and to any known features of its connectivity. For practical purposes, this was not possible for my tracing and I frequently encountered my own biases. It's unclear how much this problem arises for others who might employ teams of undergrads or otherwise outsource their tracing as it tends not to be discussed. In my experience, I know that when tracing an arbor that I knew was postsynaptic to another arbor that I had already traced I would become more attentive when the process I was tracing appeared to be drawing close to a branch of the presynaptic cell. On the other side, when I saw what appeared to be an unexpected synapse between two cells not known

to be connected I would also pay much more attention to that area. Spending increased attention to resolve important connections is not necessarily a bad thing, particularly if one is aware (and I was) of one's biases. But it should be noted anyway that more attention was paid to my synapse annotation when it involved two traced processes than when it involved only one traced process and one untraced process. (And it should be further noted that in many cases where I first noticed a synaptic input site on one cell I would later find that the presynaptic process of the other cell belonged to a neuron known to be presynaptic to the first cell). Therefore it is almost certain that some small fraction of the sites I think are synaptic are in fact not.

Tracing errors are inevitable. Tracer bias is also inevitable and leads to differences in attention being paid to certain areas versus others. Generally, counteracting error and bias is best done by increasing the number of tracers and review time.

Appendix C. A Modified staining protocol for consistent staining of leech tissue.

The following protocol is adapted from Deerinck et al., 2010, available at http://ncmir.ucsd.edu/sbfsem-protocol.pdf. *Alterations to this protocol are indicated in* ***bold*** *notes.*

1) Animals are anesthetized and dissected as routine in leech saline. For fixation preparations are transferred to a solution of 0.1M phosphate buffer containing 2.5% glutaraldehyde and 2% paraformaldehyde.

2) Target tissues are then removed and fixed for an additional 2-3 hours at 4°C.

3) Tissues are washed 5 x 3 minutes in cold cacodylate buffer containing 2mM calcium chloride (**Or use 0.1M phosphate buffer)**.

4) Right before use, a solution containing 3% potassium ferrocyanide in 0.3M cacodylate buffer with 4mM calcium chloride is combined with an equal volume of 4% aqueous osmium tetroxide (EMS). The tissues are incubated in this solution for 1 hour, on ice. **Ignore the "on ice" part here. To get the stain to evenly penetrate the tissue all the way to the center of the neuropil, we had to do microwave incubations during the staining steps. You need a laboratory microwave which can alter its power output to maintain a steady temperature as measured in a water bath within the microwave. The sample sits in a 1.5ml microcentrifuge tube in the staining solution, that tube is suspended in the water bath within the microwave. Then heat 3x (40s @35°C; 40s off). Then we let the sample sit for another 30 min at RT. This RT incubation may or may not be necessary, but the microwave incubations definitely was.**

5) While the initial osmium incubation (step 5 above) is occurring prepare the following thiocarbohydrazide (TCH) solution. This reagent needs to be fresh and available

right at the end of step 5. Add 0.1 gm thiocarbohydrazide (Ted Pella) to 10 ml ddH2O and place in a 60° C oven for 1 hour, (agitate by swirling gently every 10 minutes to facilitate dissolving). Filter this solution through a 0.22 um Millipore syringe filter right before use.

6) At the end of the first heavy metal incubation described in Step 5 (before adding the TCH) the tissues are washed with ddH2O at room temperature 5 x 3 minutes (~15 minutes total). **(Here, we did 3x (2minutes @30°C; 2minutes off) during the first wash. Then the other 2 RT washes. Again, not certain if RT additional washes matter, or if it matters whether you do the microwave during the first wash or last wash.)**

7) Tissues are then placed in the 0.22 micron Millipore filtered TCH solution for 20 minutes, at room temperature. **(Same as step 4; then 15 minutes RT).**

8) Tissues are then rinsed again 5 x 3 minutes in ddH2O at room temperature and thereafter placed in 2% osmium tetroxide (NOT osmium ferrocyanide) in ddH20 for 30 minutes, at room temperature. **(Same as step 6 for the washes, then same as step 4 for the stain, then 30 minutes RT).**

9) Following this second exposure to osmium the tissues are washed 5 x 3 minutes at room temperature in ddH2O then placed in 1% uranyl acetate (aqueous) and left in a refrigerator (~4°) overnight. **(Same as step 6 for the washes, otherwise UA stain proceeds as written).**

10) The next day, en bloc Walton's lead aspartate staining is performed. First, prepare an aspartic acid stock solution by dissolving 0.998 gm of L-aspartic acid (Sigma-Aldrich) in 250 ml of ddH2O. Note: the aspartic acid will dissolve more quickly if the pH raised to 3.8. This stock solution is stable for 1-2 months if refrigerated. To make the stain dissolve 0.066 gm of lead nitrate in 10 ml of aspartic acid stock and pH adjusted to 5.5 with 1N KOH.

The lead aspartate solution is placed in a 60°C oven for 30 minutes (no precipitate should form). The tissue is washed 5 x 3 minutes in ddH2O at room temperature and then placed in the lead aspartate solution and then returned to the oven for 30 minutes.

11) The tissues are washed 5 x 3 minutes in room temperature ddH2O and dehydrated using ice-cold solutions of freshly prepared 20%, 50%, 70%, 90%, 100%, 100% ethanol (anhydrous), 5 minutes each, then placed in anhydrous ice-cold acetone and left at room temperature for 10 minutes.

12) Tissues are placed in room temperature acetone for 10 minutes. During this time, Durcupan ACM resin (EMS) is formulated by weight as follows: 11.4 gm part A, 10 gm part B, 0.3 gm part C and 0.05-0.1 gm part D, yielding a hard resin when polymerized. The resin is mixed thoroughly samples are placed into 25% Durcupan:acetone for 2 hours, then into 50% Durcupan:acetone for 2 hours and 75% Durcupan:acetone for 2 hours.

13) Tissues are placed in 100% Durcupan overnight then into fresh 100% Durcupan for 2 hours. Tissue sections are then mounted between liquid release agent-coated glass slides (EMS) and tissue pieces are embedded in a thin layer of fresh resin in an aluminum weigh boat and place in a 60°C oven for 48 hours.

References

Angstadt, J. D., Donmoyer, J. E., & Stretton, A. O. W. (2001). The number of morphological synapses between neurons does not predict the strength of their physiological synaptic interactions: A study of dendrites in the nematode Ascaris suum. Journal of Comparative Neurology, 432(4), 512–527.

Apathy (1905). Die histologische Seite der Neuronenlehre. Journ. f. Psycholog. u. Neurolog., Bd. 5.

Atasoy, D., Betley, J. N., Li, W.-P., Su, H. H., Sertel, S. M., Scheffer, L. K., … Sternson, S. M. (2014). A genetically specified connectomics approach applied to long-range feeding regulatory circuits. Nature Neuroscience, 17(12), 1830–1839.

Bailey, C. H., & Chen, M. (1991). Morphological aspects of synaptic plasticity in Aplysia. Annals New York Academy of Sciences, 627, 181–196.

Bailey, C. H., Thompson, E. B., Castellucci, V. F., & Kandel, E. R. (1979). Ultrastructure of the synapses of sensory neurons that mediate the gill-withdrawal reflex in Aplysia. Journal of Neurocytology, 8(4), 415–44.

Berning, M., Boergens, K. M., Berning, M., Boergens, K. M., & Helmstaedter, M. (2015). SegEM : Efficient Image Analysis for High-Resolution Connectomics. Neuron, 87(6), 1193–1206.

Bhatla, N., Droste, R., Sando, S. R., Huang, A., & Horvitz, H. R. (2015). Distinct Neural Circuits Control Rhythm Inhibition and Spitting by the Myogenic Pharynx of C. elegans. Current Biology, 25(16), 2075–2089.

Bloom, F. (1992) The Gains in Brain Are Mainly in the Stain in: The Neurosciences: Paths of Discovery, I. (211-227).

Bock, D. D., Lee, W.-C. A., Kerlin, A. M., Andermann, M. L., Hood, G., Wetzel, A. W., … Reid, R. C. (2011). Network anatomy and in vivo physiology of visual cortical neurons. Nature, 471(7337), 177–182.

Briggman, K. L., Abarbanel, H. D. I., & Kristan, W. B. (2005). Optical imaging of neuronal populations during decision-making. Science (New York, N.Y.), 307(5711), 896–901.

Briggman, K. L., Helmstaedter, M., & Denk, W. (2011). Wiring specificity in the direction-selectivity circuit of the retina. Nature, 471(7337), 183–188.

Brightman, M. W., & Reese, T. S. (1969). Junctions between intimately apposed cell membranes in the vertebrate brain. Journal of Cell Biology, 40(3), 648–677.

Britten, K. H., Newsome, W. T., Shadlen, M. N., Movshon, J. A., & Celebrini, S. (1996). A relationship between behavioral choice and the visual responses of neurons in macaque MT. Visual Neuroscience, 13(01), 87–100.

Cardona, A., Saalfeld, S., Schindelin, J., Arganda-Carreras, I., Preibisch, S., Longair, M., … Douglas, R. J. (2012). TrakEM2 Software for Neural Circuit Reconstruction. PLoS ONE, 7(6), e38011.

Chalfie, Tu, Euskirchen, Ward, & Prasher. (1994). Green fluorescent protein as a marker for gene expression. Science (New York, NY), 263(5148), 802–805.

Cline, H. T., Nusbaum, M. P., & Kristan Jr., W. B. (1985). Identified GABAergic inhibitory motor neurons in the leech central nervous system take up GABA. Brain Research, 348, 359–362.

Coggeshall, R. E., & Fawcett, D. W. (1964). The Fine Structure of the Central Nervous System of the Leech, Hirudo Medicinalis. J Neurophysiol, Mar(27), 229–289.

Dani, A., Huang, B., Bergan, J., Dulac, C., & Zhuang, X. (2010). Superresolution imaging of chemical synapses in the brain. Neuron, 68(5), 843–56.

Denk, W., & Horstmann, H. (2004). Serial block-face scanning electron microscopy to reconstruct three-dimensional tissue nanostructure. PLoS Biology, 2(11), e329.

DeRiemer, S. A., & Macagno, E. R. (1981). Light microscopic analysis of contacts between pairs of identified leech neurons with combined use of horseradish peroxidase and lucifer yellow. J Neurosci, 1(6), 650–657.

Emmons, S. W. (2015). The beginning of connectomics: a commentary on White et al. (1986) “The structure of the nervous system of the nematode Caenorhabditis elegans”. Philosophical Transactions of the Royal Society of London. Series B, Biological Sciences, 370(1666).

Enjin, A., Suh, G. S. B., Bargmann, C. I., Marder, E., Mathuru, A. S., Kibat, C., … Jesuthasan, S. (2013). From the connectome to brain function. Current Biology, 22(6), 538–544.

Fan, R.-J., Marin-Burgin, A., French, K. a, & Otto Friesen, W. (2005). A dye mixture (Neurobiotin and Alexa 488) reveals extensive dye-coupling among neurons in leeches; physiology confirms the connections. Journal of Comparative Physiology. A, Neuroethology, Sensory, Neural, and Behavioral Physiology, 191, 1157–1171.

Fernández, J. (1978). Structure of the leech nerve cord: distribution of neurons and organization of fiber pathways. Journal of Comparative Neurology, 180, 165–191.

Frank, E., Jansen, J. K. S., & Rinvik, E. (1975). A multisomatic axon in the central nervous system of the leech. Journal of Comparative Neurology, 159, 1–13.

Friesen, W. (1989a). Neuronal control of leech swimming movements. Journal of Comparative Physiology A, 195–203.

Friesen, W. (1989b). Neuronal control of leech swimming movements. Journal of Comparative Physiology A, 208, 195–203.

Friesen, W. O., Poon, M., & Stent, G. S. (1978). Neuronal control of swimming in the medicinal leech. IV. Identification of a network of oscillatory interneurones. The Journal of Experimental Biology, 75, 25–43.

Goaillard, J., Taylor, A. L., Schulz, D. J., & Marder, E. (2010). Functional consequences of animal-to-animal variation in circuit parameters, 12(11), 1424–1430.

Golgi, C. (1873). Sulla sostanza grigia del cervello. Gazz. Med. Ital. Lombardia, 6, 244–246.

Granzow, B., Friesen, W. O., & Kristan, W. B. (1985). Physiological and morphological analysis of synaptic transmission between leech motor neurons. J. Neuroscience, 5(8), 2035–2050.

Gray, E. G. (1959). Axo-somatic and axo-dendritic synapses of the cerebral cortex. Journal of Anatomy, 93, 420–433.

Gray, E. G., & Guillery, R. W. (1963). An electron microscopical study of the ventral nerve cord of the leech. Zeitschrift Fur Zellsforschung, 60, 826–849.

Harris, K. M., Perry, E., Bourne, J., Feinberg, M., Ostroff, L., & Hurlburt, J. (2006). Uniform Serial Sectioning for Transmission Electron Microscopy. Journal of Neuroscience, 26(47), 12101–12103.

Helmstaedter, M. (2013). Cellular-resolution connectomics: challenges of dense neural circuit reconstruction. Nature Methods, 10(6), 501–507.

Helmstaedter, M., Briggman, K. L., & Denk, W. (2011). High-accuracy neurite reconstruction for high-throughput neuroanatomy. Nature Neuroscience, 14(8), 1081–1088.

Helmstaedter, M., Briggman, K. L., Turaga, S. C., Jain, V., Seung, H. S., & Denk, W. (2013). Connectomic reconstruction of the inner plexiform layer in the mouse retina. Nature, 500(7461), 168–74.

Hillman, H., & Deutsch, K. (1978). Area changes in slices of rat brain during preparation for histology or electron microscopy. J Microsc, 114(1), 77–84.

Hua, Y., Laserstein, P., & Helmstaedter, M. (2015). Large-volume en-bloc staining for electron microscopy-based connectomics. Nature Communications, 6, 7923.

Imai, J. H., & Meinertzhagen, I. A. N. A. (2007). Neurons of the Ascidian Larval Nervous System in Ciona intestinalis : II ., 352(October 2006), 335–352.

Jarrell, T. a., Wang, Y., Bloniarz, a. E., Brittin, C. a., Xu, M., Thomson, J. N., … Emmons, S. W. (2012). The Connectome of a Decision-Making Neural Network. Science, 337(6093), 437–444.

Kilman, V. L., & Marder, E. (1996). Ultrastructure of the stomatogastric ganglion neuropil of the crab, Cancer borealis. The Journal of Comparative Neurology, 374(3), 362–75.

Kim, J. S., Greene, M. J., Zlateski, A., Lee, K., Richardson, M., Turaga, S. C., … Seung, H. S. (2014). Space-time wiring specificity supports direction selectivity in the retina. Nature, 509(7500), 331–6.

King, D. G. (1976). Organization of crustacean neuropil. II. Distribution of synaptic contacts on identified motor neurons in lobster stomatogastric ganglion. J Neurocytol, 5(2), 239–266.

Kinney, J. P., Spacek, J., Bartol, T. M., Bajaj, C. L., Harris, K. M., & Sejnowski, T. J. (2013). Extracellular sheets and tunnels modulate glutamate diffusion in hippocampal neuropil. Journal of Comparative Neurology, 521(2), 448–464.

Klausberger, T. (2009). GABAergic interneurons targeting dendrites of pyramidal cells in the CA1 area of the hippocampus. European Journal of Neuroscience, 30(6), 947–957.

Knott, G., Marchman, H., Wall, D., & Lich, B. (2008). Serial Section Scanning Electron Microscopy of Adult Brain Tissue Using Focused Ion Beam Milling. Journal of Neuroscience, 28(12), 2959–2964.

Korogod, N., Petersen, C. C., & Knott, G. W. (2015). Ultrastructural analysis of adult mouse neocortex comparing aldehyde perfusion with cryo fixation. eLife, 4, 1–17.

Kremer, J. R., Mastronarde, D. N., & McIntosh, J. R. (1996). Computer visualization of three-dimensional image data using IMOD. Journal of Structural Biology, 116(1), 71–76.

Kristan, W. B., & Calabrese, R. L. (1976). Rhythmic swimming activity in neurones of the isolated nerve cord of the leech. The Journal of Experimental Biology, 65(3), 643–68.

Kristan, W. B., Stent, G. S., & Ort, C. a. (1974). Neuronal control of swimming in the medicinal leech - I. Dynamics of the swimming rhythm. Journal of Comparative Physiology ??? A, 94(2), 97–119.

Kuffler, D. P., Nicholls, J., & Drapeau, P. (1987). Transmitter localization and vesicle turnover at a serotoninergic synapse between identified leech neurons in culture. The Journal of Comparative Neurology, 256(4), 516–526.

Lacalli, T. C. (2009). Serial EM analysis of a copepod larval nervous system: Naupliar eye, optic circuitry, and prospects for full CNS reconstruction. Arthropod Structure & Development, 38(5), 361–75.

Lam, S. S., Martell, J. D., Kamer, K. J., Deerinck, T. J., Ellisman, M. H., Mootha, V. K., & Ting, A. Y. (2014). Directed evolution of APEX2 for electron microscopy and proximity labeling. Nature Methods, 12(1), 51–54.

Laverack, M. S. (1969). Mechanoreceptors, photoreceptors and rapid conduction pathways in the leech, Hirudo medicinalis. The Journal of Experimental Biology, 50(1), 129–140.

Lehmann, T., Heß, M., Wanner, G., & Melzer, R. R. (2014). Dissecting a neuron network: FIB-SEM-based 3D-reconstruction of the visual neuropils in the sea spider Achelia langi (Dohrn, 1881) (Pycnogonida). BMC Biology, 12, 59.

Leinwand, S. G., & Chalasani, S. H. (2013). Neuropeptide signaling remodels chemosensory circuit composition in Cainorahbditis elegans. Nature N, 16(10), 1461–1467.

Lent, C. M., Zundel, D., Freedman, E., & Groome, J. R. (1991). Serotonin in the leech central nervous system: anatomical correlates and behavioral effects. Journal of Comparative Physiology. A, Sensory, Neural, and Behavioral Physiology, 168(2), 191–200.

Levshin, L. V. (1978). Serial Synapses in Aplysia. Journal of Neurobiology, 9(4), 325–328.
Livet, J., Weissman, T. a, Kang, H., Draft, R. W., Lu, J., Bennis, R. a, … Lichtman, J. W. (2007). Transgenic strategies for combinatorial expression of fluorescent proteins in the nervous system. Nature, 450(7166), 56–62.

Lo, L., & Anderson, D. J. (2011). A Cre-Dependent, Anterograde Transsynaptic Viral Tracer for Mapping Output Pathways of Genetically Marked Neurons. Neuron, 72(6), 938–950.

Lockery, S. R., & Kristan, W. B. (1990a). Distributed Processing of Sensory Information I . Input-Output Relations of the Local Bending in the Leech . Reflex. The Journal of Neuroscience, 10(6)(June), 1811–1815.

Lockery, S. R., & Kristan, W. B. (1990b). Distributed Processing of Sensory Information in the Leech . II . Identification of Interneurons Contributing Reflex IN-l. The Journal of Neuroscience, 10(6)(June), 1816–1829.

Lytton, W. W., & Kristan, W. B. (1989). Localization of a leech inhibitory synapse by photo-ablation of individual dendrites. Brain Research, 504(1), 43–8.

Macagno, E. R. (1980). Number and distribution of neurons in leech segmental ganglia. The Journal of Comparative Neurology, 190(2), 283–302.

Magni, F., & Pellegrino, M. (1978). Patterns of activity and the effects of activation of the fast conducting system on the behaviour of unrestrained leeches. J Exp Biol., 76, 123–135.

Maranto, A. R. (1982). Neuronal mapping: a photooxidation reaction makes Lucifer yellow useful for electron microscopy. Science (New York, N.Y.), 217(4563), 953–955.

Marder, E. (2012). Neuromodulation of neuronal circuits: back to the future. Neuron, 76(1), 1–11.

Marin-Burgin, A., Eisenhart, F. J., Baca, S. M., Kristan, W. B., & French, K. a. (2005). Sequential development of electrical and chemical synaptic connections generates a specific behavioral circuit in the leech. The Journal of Neuroscience : The Official Journal of the Society for Neuroscience, 25(10), 2478–89.

Mikula, S., & Denk, W. (2015). High-resolution whole-brain staining for electron microscopic circuit reconstruction. Nature Methods, 12(6), 541–546.

Miller, E. W., Lin, J. Y., Frady, E. P., Steinbach, P. A., Kristan, W. B., & Tsien, R. Y. (2012). Optically monitoring voltage in neurons by photo-induced electron transfer through molecular wires. Proceedings of the National Academy of Sciences of the United States of America, 109(6), 2114–9.

Muller, K. J. (1979). Synapses between neurones in the central nervous system of the leech. Biological Reviews of the Cambridge Philosophical Society, 54(2), 99–134.

Muller, K. J., & McMahan, U. J. (1976). The shapes of sensory and motor neurones and the distribution of their synapses in ganglia of the leech: a study using intracellular injection of horseradish peroxidase. Proceedings of the Royal Society of London, Series B, 194(1117), 481–499.

Muller, K. J., & Scott, S. A. (1981). Transmission at a “direct” electrical connexion mediated by an interneurone in the leech. J. Physiology, 311, 565–583.

Nakano, H., Nakajima, Y., & Amemiya, S. (2009). Nervous system development of two crinoid species, the sea lily Metacrinus rotundus and the feather star Oxycomanthus japonicus. Development Genes and Evolution, 219(11-12), 565–76.

Narayanan Kasthuri, A., Jeffrey Hayworth, K., Raimund Berger, D., Eldin Priebe, C., Pfister, H., William Lichtman, J., … Lewis Sussman, D. (2015). Saturated Reconstruction of a Volume of Neocortex. Cell, 162, 648–661.

Nässel, D. R., Meyer, E. P., & Klemm, N. (1985). Mapping and ultrastructure of serotonin-immunoreactive neurons in the optic lobes of three insect species. The Journal of Comparative Neurology, 232(2), 190–204.

Nicholls, J. G., & Baylor, D. a. (1968). Specific modalities and receptive fields of sensory neurons in CNS of the leech . Specific Modalities and Receptive Fields of Sensory Neurons in CNS of the Leech. J Neurophysiol, 31, 740–756.
Nicholls, J. G., Liu, Y., Payton, B., & Kuffler, D. P. (1990). The specificity of synapse formation by identified leech neurons in culture. J Exp Biol., 153, 141–154.

Nicholls, J. G., & Purves, D. (1970). Monosynaptic chemical and eletrical connexions between sensory and motor cells in the central nervous system of the leech. J. Physiology, 209, 647–667.

Ohyama, T., Schneider-Mizell, C. M., Fetter, R. D., Aleman, J. V., Franconville, R., Rivera-Alba, M., … Zlatic, M. (2015). A multilevel multimodal circuit enhances action selection in Drosophila. Nature, 520(7549), 633–9.

Ort, C. A., Kristan, W. B., & Stent, G. S. (1974). Neuronal Control of Swimming in the Medicinal Leech II. Identification and Connections of Motor Neurons. J. Compl. Physiology, 94, 121–154.

Purves, D., & Mcmahan, U. E. L. J. (1972). The distribution of synapses on a neuron in the central nervous system of the leech: An Electron Microscope Study after the Injection of the Fluorescent Dye Procion Yellow, 55, 205–220.

Randel, N., Asadulina, A., Bezares-Calderón, L. A., Verasztó, C., Williams, E. A., Conzelmann, M., … Jékely, G. (2014). Neuronal connectome of a sensory-motor circuit for visual navigation. eLife, 3, 1–22.

Randel, N., Shahidi, R., Verasztó, C., Bezares-Calderón, L. a., Schmidt, S., & Jékely, G. (2015). Inter_individual stereotypt of Platynereis larval visual connectome. eLIFE, (June), 1–15.

Reynolds, S. a, French, K. a, Baader, a, & Kristan, W. B. (1998). Staging of middle and late embryonic development in the medicinal leech, Hirudo medicinalis. The Journal of Comparative Neurology, 402(2), 155–67.

Sahley, C. L., Modney, B. K., Boulis, N. M., & Muller, K. J. (1994). The S Cell: An Interneuron Essential for Sensitization and Full Dishabituation of Leech Shortening. The Journal of Neuroscience, 14(November), 6715–6721.

Shaw, B. K., & Kristan Jr., W. B. (1995). The whole-body shortening reflex of the medicinal leech: motor pattern, sensory basis, and interneuronal pathways. Journal of Comparative Physiology A, 177(6), 667–681.

Sherrington, C. S. (1906). The Integrative Action of the Nervous System. Charles Scribner's Sons, New York.

Shomrat, T., & Levin, M. (2013). An automated training paradigm reveals long-term memory in planarians and its persistence through head regeneration. Journal of Experimental Biology, 216(20), 3799–3810.

Sporns, O., Tononi, G., & Kötter, R. (2005). The Human Connectome: A Structural Description of the Human Brain. PLoS Computational Biology, 1(4), e42.

Stent, G. S., Kristan, W. B., Friesen, W. O., Ort, C. a, Poon, M., & Calabrese, R. L. (1978). Neuronal generation of the leech swimming movement. Science (New York, N.Y.), 200(4348), 1348–57.

Takemura, S., Bharioke, A., Lu, Z., Nern, A., Vitaladevuni, S., Rivlin, P. K., … Chklovskii, D. B. (2013). A visual motion detection circuit suggested by Drosophila connectomics. Nature, 500(7461), 175–181.

Trueta, C., Kuffler, D. M. P., & De-Miguel, F. F. (2012). Cycling of dense core vesicles involved in somatic exocytosis of serotonin by leech neurons. Frontiers in Physiology, 3 JUN(June), 1–13.

Wadepuhl, M., Schäffner, K., & Eberle, R. (1990). An unusual cell in the central nervous system of Hirudo medicinalis L.: a neuron with ribbon and flags. Cell and Tissue Research, 259, 247–254.

Wanner, A. A., Kirschmann, M. A., & Genoud, C. (2015). Challenges of microtome-based serial block-face scanning electron microscopy in neuroscience. Journal of Microscopy, 259(2), 137–142.

Watson, a H., & Burrows, M. (1983). The morphology, ultrastructure, and distribution of synapses on an intersegmental interneuron of the locust. The Journal of Comparative Neurology, 214(2), 154–169.

Watson, A. H., & Burrows, M. (1982). The ultrastructure of identified locust motor neurones and their synaptic relationships. J Comp Neurol, 205(4), 383–397.

White, J. (1986). The nervous system of the nematode c. elegans. The Philosophical Transactions of the Royal Society, London.

White, J. G., Southgate, E., Thomson, J. N., & Brenner, S. (1986). The Structure of the Nervous System of the Nematode Caenorhabditis elegans: The Mind of a Worm. Philosophical Transactions of the Royal Society B: Biological Sciences, 314(1165), 1–340.

Wickersham, I. R., Lyon, D. C., Barnard, R. J. O., Mori, T., Conzelmann, K., Young, J. a T., … Neurons, G. T. (2007). Monosynaptic Restriction of Transsynaptic Tracing from Single, Genetically Targeted Neurons. Neuron, 53(5), 639–647.

Wilke, S. a, Raam, T., Antonios, J. K., Bushong, E. a, Koo, E. H., Ellisman, M. H., & Ghosh, A. (2014). Specific disruption of hippocampal mossy fiber synapses in a mouse model of familial Alzheimer's disease. PloS One, 9(1), e84349.

Wilke, S. A., Antonios, J. K., Bushong, E. A., Badkoobehi, A., Malek, E., Hwang, M., … Ghosh, A. (2013). Deconstructing Complexity: Serial Block-Face Electron Microscopic Analysis of the Hippocampal Mossy Fiber Synapse. Journal of Neuroscience, 33(2), 507–522.